



# Enhancing Long-Term Vegetation Monitoring in Australia: A New Approach for Harmonising and Gap-Filling AVHRR and MODIS NDVI

5 Chad. A. Burton<sup>1</sup>, Sami. W. Rifai<sup>2</sup>, Luigi. J. Renzullo<sup>3</sup> and Albert. I.J.M. Van Dijk<sup>1</sup>

<sup>1</sup> Fenner School of Environment & Society, Australian National University, Canberra, ACT, Australia.

<sup>2</sup> School of Biological Sciences, The University of Adelaide, Adelaide SA, Australia.

<sup>3</sup> Bureau of Meteorology, Hydrology Science, Canberra, Australia

10

**Correspondence:** Chad Burton (chad.burton@anu.edu.au)

## Abstract.

Long-term, reliable datasets of satellite-based vegetation condition are essential for understanding  
15 terrestrial ecosystem responses to global environmental change, particularly in Australia which is  
characterised by diverse ecosystems and strong interannual climate variability. We comprehensively  
evaluate several existing global AVHRR NDVI products for their suitability for long-term vegetation  
monitoring in Australia. Comparisons with MODIS NDVI highlight significant deficiencies,  
particularly over densely vegetated regions. Moreover, all the assessed products failed to adequately  
20 reproduce inter-annual variability in the pre-MODIS era as indicated by Landsat NDVI anomalies. To  
address these limitations, we propose a new approach to calibrating and harmonising NOAA's Climate  
Data Record AVHRR NDVI to MODIS MCD43A4 NDVI for Australia using a gradient-boosting  
decision tree ensemble method. Two versions of the datasets are developed, one incorporating climate  
data in the predictors ('AusENDVI-clim': **Australian Empirical NDVI-climate**) and another  
25 independent of climate data ('AusENDVI-noclim'). These datasets, spanning 1982-2013 at a spatial  
resolution of 0.05°, exhibit strong correlation and low relative errors compared to MODIS NDVI,  
accurately reproducing seasonal cycles over densely vegetated regions. Furthermore, they closely  
replicate the interannual variability in vegetation condition in the pre-MODIS era. A reliable method



for gap-filling the AusENDVI record is also developed that leverages climate, atmospheric CO<sub>2</sub>  
30 concentration, and woody cover fraction predictors. The resulting synthetic NDVI dataset shows  
excellent agreement with observations. Finally, we provide a complete 41-year dataset where gap filled  
AusENDVI from January 1982 to February 2000 is seamlessly joined with MODIS NDVI from March  
2000 to December 2022. Analysing 40-year per-pixel trends in Australia's annual maximum NDVI  
35 NDVI are identified, underscoring the dataset's potential to address crucial questions regarding  
changing vegetation phenology and its drivers. The AusENDVI dataset can be used for studying  
Australia's changing vegetation dynamics and downstream impacts on terrestrial carbon and water  
cycles, and provides a reliable foundation for further research into the drivers of vegetation change.  
AusENDVI is open access and available at <https://doi.org/10.5281/zenodo.10802704> (Burton, 2024).

## 40 **1 Introduction**

Australia is undergoing long-term changes to its climate that are impacting terrestrial vegetation, with  
attendant serious implications for ecosystem functioning, carbon and water cycles, and agriculture  
(Hoffmann et al., 2019; Canadell et al., 2021; Head et al., 2014; Hughes, 2011; Steffen et al., 2011;  
Rifai et al., 2022; Ukkola et al., 2016; Donohue et al., 2009). Long-term, reliable datasets that chart the  
45 land surface response to climate change are crucial if we are to identify, understand, and respond to  
ongoing terrestrial ecosystem change (Giglio and Roy, 2020; Piao et al., 2019). One of the primary  
means Earth System Science has to trace long-term vegetation change is the Normalised Difference  
Vegetation Index (NDVI), a widely used satellite-derived indicator of vegetation condition owing to its  
close relation to vegetation productivity. NDVI provides an efficient means for mapping and monitoring  
50 vegetation condition at continental scales. In Australia, the need for very long records of NDVI to  
understand change is amplified by strong variability at both interannual and interdecadal time scales,  
and ecosystems that are often driven by periodic, but non-seasonal phenological drivers (Moore et al.,  
2016; Chambers et al., 2013; Ma et al., 2013; Beringer et al., 2022).



The MODerate resolution Imaging Spectroradiometer (MODIS) NDVI record ( $NDVI_{MODIS}$ ) is generally considered the most reliable global scale dataset due to its high quality radiometrics and accurate georeferencing. Unfortunately, the MODIS record only begins in March 2000 (Vermote et al., 2002). The Advanced Very High-Resolution Radiometer (AVHRR) NDVI record ( $NDVI_{AVHRR}$ ) is the longest contiguous series of satellite data, starting in July 1981, but has several well-known problems owing to a lack of on-board calibration for visible wavelengths, sensor orbital drift, and sensor degradation, making it unreliable for detecting relatively subtle trends over multiple decades (Tucker et al., 2005; Privette et al., 1995; Gorman and McGregor, 1994). Several exemplary global  $NDVI_{AVHRR}$  products attempt to ameliorate these issues. For example, the Global Inventory Modelling and Mapping Studies version 3 ( $NDVI_{GIMMS3g}$ ) applies Bayesian analysis with Sea-Viewing Wide Field-of-View Sensor NDVI as evidence information to reduce sensor transition discontinuities and increase the dynamic range of  $NDVI_{AVHRR}$  (Pinzon and Tucker, 2014), while the NOAA Climate Data Record ( $NDVI_{CDR}$ ) applies a suite of corrections to create a consistent surface reflectance product (Franch et al., 2017), among others (Table 1). However, despite substantial progress, errors and biases in these NDVI products have led to inconsistent findings on global greening (Wang et al., 2022; Wang et al., 2021; Cortés et al., 2021; Frankenberg et al., 2021; Fensholt and Proud, 2012), discrepancies in vegetation seasonality between datasets (Ye et al., 2021), and persistent temporal inconsistencies (Tian et al., 2015; Giglio and Roy, 2020). Recently, Li et al. (2023) developed a new global  $NDVI_{AVHRR}$  product, ‘GIMMS-PKU’ ( $NDVI_{GIMMS-PKU}$ ), which effectively calibrates the  $NDVI_{GIMMS3g}$  archive to the Landsat record using machine learning techniques, and ‘GIMMS-PKU-consolidated’ ( $NDVI_{PKU-consolidated}$ ) which harmonises  $NDVI_{GIMMS-PKU}$  to  $NDVI_{MODIS}$  (Table 1), but which has yet to be extensively assessed in the literature (Li et al., 2023).

As much as possible, any NDVI product that exploits the AVHRR and MODIS record to acquire an accurate >40-year record of vegetation condition should attempt to integrate the two seamlessly while also performing well in the pre-MODIS AVHRR era (1982-2000). Performance should be judged on how well seasonal cycles are represented along with interannual and interdecadal variability, as both seasonal and longer-term fluctuations in vegetation conditions have important ramifications for carbon and water cycles (Ma et al., 2015). An effectively calibrated, harmonised, and gap-filled dataset can



form the basis for studying the biogeophysical impacts of global change and meteorological variability on Australia's terrestrial vegetation. With that in mind, the objectives of this study are as follows:

- 85 • To investigate existing  $NDVI_{AVHRR}$  datasets to determine their suitability for long-term vegetation monitoring in Australia by both comparing their consistency with  $NDVI_{MODIS}$  during the 2000-2013 overlap period, and with Landsat NDVI ( $NDVI_{Landsat}$ ) anomalies from 1988-2000.
- 90 • Having established limitations with the existing datasets, calibrate and harmonise  $NDVI_{AVHRR}$  to  $NDVI_{MODIS}$  solely over Australia at the highest spatial resolution possible. The final dataset should contain the harmonised  $NDVI_{AVHRR}$  from January 1982 to February 2000, where it seamlessly joins with the superior  $NDVI_{MODIS}$  timeseries, resulting in a reliable 40-year record of vegetation condition for Australia. We will call this time series “AusENDVI” (for Australian Empirical NDVI;  $NDVI_{AusE}$ )
- 95 • To develop a reliable method for gap filling the  $NDVI_{AusE}$  record caused by sensor transitions issues and long periods of missing or suspect data acquisition.
- To demonstrate the utility of this new dataset by exploring NDVI phenology trend analysis, including long-term trends in the value and timing of annual maximum NDVI across the Australian continent.

## 2 Materials and Methods

### 100 2.1 Datasets

Features of all datasets used for either the intercomparison of NDVI products or in the modelling framework are listed in Table 1. For comparisons between NDVI datasets, finer resolution datasets were resampled to match the coarsest grid (i.e., GIMMS,  $1/12^\circ$  or  $\sim 8$  km over Australia) using averaging or nearest-neighbour techniques. Wherever datasets are compared, data gaps are matched  
105 between all participating datasets. We chose Landsat's TM and ETM+ (Table 1) as the sensor for comparison in the pre-MODIS era owing to the international efforts to produce a relatively high geometric and radiometric accuracy for its generation, and its lack of sensor transitions (Beck et al.,



2011). The chosen surface reflectance Landsat product, Digital Earth Australia’s Landsat NBAR  
(Nadir-corrected BRDF Adjusted Reflectance, where BRDF stands for Bidirectional reflectance  
110 distribution function) product is calibrated to Australia’s environment using the MODTRAN 4 radiative  
transfer model and BRDF shape functions derived from MODIS (Li et al., 2010).

For the development of the Australian NDVI dataset, we relied on the NOAA NDVI<sub>CDR</sub> product  
(Franch et al., 2017) as the input dataset. This was principally because of its higher spatial resolution  
than the other datasets (~5 km), its lack of gap filling, extensive atmospheric corrections, and its BRDF-  
115 based correction of view-angle effects (Ma et al., 2019). As the target dataset, we derived NDVI from  
the MODIS MCD43A4 surface reflectance NBAR product (NDVI<sub>MCD43A4</sub>). This reflectance product  
was chosen because of its similar set of atmospheric corrections when compared with NDVI<sub>CDR</sub> and  
Landsat NBAR, and its use of both the Terra and Aqua instruments which extends its temporal extent  
back to March 2000 (Schaaf and Wang, 2015).

120 All additional input data used in NDVI estimation were temporally aggregated to monthly  
values by calculating medians and spatially reprojected onto a common 0.05° geographic grid. In  
addition to filtering based on the quality assurance band additional criteria were applied to minimise the  
impact of temporal discontinuities in the NDVI<sub>CDR</sub> record that may arise from orbital decay or sensor  
degradation. Monthly NDVI<sub>CDR</sub> values based on fewer than two observations per month were  
125 discarded, along with any values for which the coefficient of variation in daily retrievals for a given  
month was greater than 50 %. Anomalies in NDVI, solar-zenith-angle, and time-of-acquisition that  
were greater than 3.5 standard deviations were also discarded (based on a 1982-2013 climatology).  
Following the advice of Tian et al. (2015), data for several problematic sensor transition periods were  
discarded (September 1984 - April 1985, July 1988 - September 1989, and July 1993 - December 1994).  
130 After filtering, the continental average fraction of available data is 0.79, meaning on average 79 % of  
the monthly time-steps between 1982-2013 are preserved (Figure A1).

**Table 1: Details of the datasets used in, and produced by, this study.**

Dataset & Abbreviation	Native spatial resolution, temporal range, and details	Data Source & Reference
------------------------	--	-------------------------



AVHRR Climate Data Record NDVI and Surface Reflectance; NDVICDR	0.05°, January 1982 to December 2013. Surface reflectance product used for the time-of-day and solar zenith angle.	Version 5, downloaded from Google Earth Engine, (Franch et al., 2017)
MODIS MCD43A4 NDVI; NDVIMCD43A4	~500m, March 2000 to December 2022. Calculate from the combined Terra and Aqua MCD43A4 surface reflectance NBAR product.	Version 6 downloaded from Google Earth Engine (Schaaf and Wang, 2015)
AVHRR GIMMS3g NDVI; NDVIGIMMS3g	1/12°, 1982-2013. AVHRR NDVI with sensor transition discontinuities reduced with Bayesian analysis.	Version 1.0 downloaded from Google Earth Engine (Pinzon and Tucker, 2014)
AVHRR GIMMS PKU NDVI; NDVIPKU, NDVIPKU-consolidated	1/12°, 1982-2022. Two variations, ‘GIMMS-PKU-solely’ and ‘GIMMS-PKU-consolidated’, the latter is harmonised with MODIS.	Version 1.2 downloaded from <a href="https://zenodo.org/records/8253971">https://zenodo.org/records/8253971</a> (Li et al., 2023)
Digital Earth Australia’s Landsat NDVI (NBAR); NDVILandsat	30m, 1987-2012, NDVI calculated from an Australian-specific Landsat 5 & 7 surface reflectance NBAR product.	Collection 3, <a href="https://docs.dea.ga.gov.au/data/product/dea-surface-reflectance-nbar-landsat-5-tm/">https://docs.dea.ga.gov.au/data/product/dea-surface-reflectance-nbar-landsat-5-tm/</a> (Li et al., 2010)
AusENDVI-clim and AusENDVI-noclim; NDVIAusE-clim, NDVIAusE-noclim	0.05°, 1982-2013. Calibrated and harmonised NDVI for Australia using machine-learning techniques. The ‘clim’ version of the dataset includes climate variables in the feature set, the ‘noclim’ version does not.	This study
Synthetic NDVI; NDVISYN	0.05°, 1982-2022. A machine-learning derived synthetic NDVI built using climate, CO <sub>2</sub> , and landscape features, and trained on NDVIAusE-clim and NDVIMCD43A4.	This study
ANU Climate: <ul style="list-style-type: none"> <li>• Average Air Temp; Tavg</li> <li>• Vapour Pressure Deficit; VPD</li> <li>• Incoming Shortwave Radiation; srad</li> <li>• Total Precipitation; rain</li> </ul>	~1 km, 1982-2022. Gridded climate products based on topographically conditional spatial interpolation of weather stations.	ANUClimate, <a href="https://dapds00.nci.org.au/thredds/catalogs/gh70/catalog.html">https://dapds00.nci.org.au/thredds/catalogs/gh70/catalog.html</a> (Hutchison et al., 2014)
Atmospheric CO <sub>2</sub> concentration	N/A., 1982-2022. Extracted from the Cape Grim Baseline Air Pollution Station in Tasmania, Australia. De-seasonalised using a 12-month running mean.	CSIRO Environment and the Australian Bureau of Meteorology (Kennaook / Cape Grim Baseline Air Pollution Station). <a href="https://capegrim.csiro.au/">https://capegrim.csiro.au/</a>
Woody Cover Fraction; WCF	25m, 1982-2022. A per-pixel estimate of woody cover fraction across Australia. Annual product for 1990-2022. A five-year average from 1990-1995 was used to extend the	<a href="https://dapds00.nci.org.au/thredds/catalog/ub8/au/LandCover/DEA_ALC/catalog.html">https://dapds00.nci.org.au/thredds/catalog/ub8/au/LandCover/DEA_ALC/catalog.html</a>



135

## 2.2 Assessment of existing NDVI products

We compared  $NDVI_{AVHRR}$  datasets with  $NDVI_{MCD43A4}$  for the overlapping period from March 2000 to December 2013. Per-pixel Pearson correlation ( $r$ ) and coefficient of variation (CV; root mean square error divided by the long-term mean  $NDVI_{MCD43A4}$ ) describe the agreement between datasets, in addition to comparison of the long-term seasonal cycle. Next,  $NDVI_{AVHRR}$  datasets were compared to annual rolling mean standardised anomalies of  $NDVI_{Landsat}$  for 1988-2000 to assess how well each product reproduces inter-annual variability in vegetation condition in the pre-MODIS era.

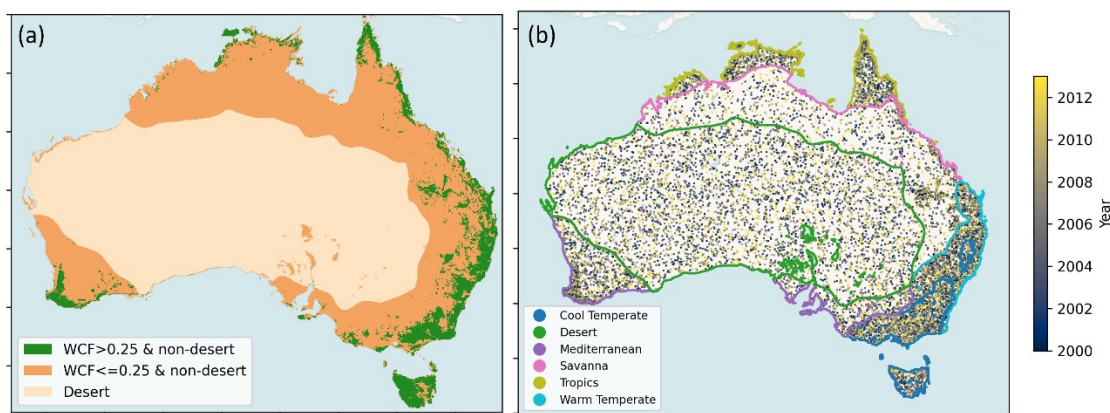
## 2.3 Calibration and harmonisation

During extensive preliminary testing gradient-boosting decision tree ensembles (GBM), random forest, and generalised additive models were assessed for their ability to calibrate and harmonise  $NDVI_{CDR}$  with  $NDVI_{MCD43A4}$ . The GBM outperformed the other approaches. Two classes of models and datasets were built: one that utilises climate data (hereafter referred to as ‘clim’ models) in the feature set to achieve the best possible agreement between  $NDVI_{CDR}$  and  $NDVI_{MCD43A4}$ . The second excludes climate features (hereafter, ‘noclim’ model) while still achieving satisfactory results. When examining drivers of change, users of these datasets may prefer to use the no-climate model to limit potential circularities in attribution of the drivers of change. During testing, climate variables were identified as useful features for both improving predictions in the heavily forested regions where there was little to no agreement between  $NDVI_{MCD43A4}$  and  $NDVI_{AVHRR}$ , and for capturing interannual variability. The ‘noclim’ models used the following features: solar-zenith-angle (SZEN), time-of-acquisition (TOD), month-of-year, latitude, and  $NDVI_{MCD43A4}$  summary percentiles (0.05, 0.5, and 0.95). The ‘clim’ models used the same variables, plus incoming solar radiation, rainfall, temperature, and vapour pressure deficit. Fractional anomalies of the climate features are also included, along with cumulative three- and six-month rainfall. Testing revealed the best results were obtained by generating three separate models



for areas with high and low woody cover fraction (WCF), and for the desert bioclimatic region (Figure  
160 1a). The long-term mean of WCF was extracted from Liao et al. (2020) and a threshold of  $WCF=0.25$   
was used to separate regions with a high woody canopy cover. This threshold was chosen as it  
approximately delineated those regions with the poorest correspondence between  $NDVI_{CDR}$  and  
 $NDVI_{MCD43A4}$  (Figure 2e-h).

In the high and low WCF regions, training and testing samples were drawn using an equalised  
165 random sampling stratification where a total of 30,000 samples were extracted in equal measure from  
the five remaining bioclimatic regions after excluding the desert (i.e., 6,000 samples per region).  
Bioclimatic regions were identical to those defined by Haverd et al. (2013) (Figure 1b). In the desert  
region, samples were drawn using a simple random approach. In all modelling domains, samples were  
drawn from any point in time across the overlap period, and 5,000 samples were randomly separated as  
170 an independent validation set, leaving 25,000 samples for training.



175 **Figure 1:** a) Regions delineating the spatial extent of the three modelling domains: desert, low woody cover fraction (WCF) and high WCF. b) The distribution of all independent validation points used to assess the model fits across the three modelling domains in (a); points are coloured by the year they are drawn from. Figure is overlaid with outlines of the six bioclimatic regions used to both stratify training points and for aggregating trends in later analysis.

Cross validation for model hyperparameter optimization was conducted using a nested cross-validation approach with five outer splits and three inner splits (Cawley and Talbot, 2010). Mean  
180 absolute error (MAE) and the coefficient of determination ( $R^2$ ) are reported as indicators of the goodness of fits. To understand which explanatory variables most impacted predictions, feature



importance plots were produced using the Shapley Additive Explanations (SHAP) Python library (Lundberg and Lee, 2017).

## 2.3 Gap-filling

185 At times there are long gaps in AVHRR data acquisition over Australia. For example, 1994 is entirely  
missing, and during sensor transition periods the data becomes unreliable for several months before and  
after the transitions (Tian et al., 2015). Furthermore, owing to the nature of Australia's prevailing  
weather systems such as the tropical monsoon, it is not uncommon to have whole geographic regions  
missing for a given month. This undermines the typical approaches to gap filling that work well when  
190 either the temporal gap is short (e.g., temporal interpolation methods using linear or polynomial fits), or  
the spatial pattern of gaps are quasi-random such as from scattered cloud cover (spatial interpolation  
methods such as nearest neighbour, kriging etc.) (Bessenbacher et al., 2022; Shen et al., 2015). Gap-  
filling with a climatology can often mask important interannual variability at key times – such as  
anomalously high rainfall periods associated with La Niñas when enhanced cloud cover masks large-  
195 scale greening events across Australia's northern tropical savanna. To avoid this we used well  
established machine learning approaches that have been developed to fill gaps in univariate data  
(Gerber et al., 2018; Zeng et al., 2014). Here, we develop a two-stage process for gap-filling. Firstly, to  
fill short temporal gaps, the time series is split into a climatology and anomaly series and linear  
temporal interpolation is applied to the anomalies for a maximum of one time-step (i.e., one month).  
200 Longer temporal gaps are replaced with a synthetic NDVI dataset generated using a similar GBM  
machine learning method as the harmonisation and is described further below.

### 2.3.1 Synthetic NDVI

Training samples were extracted from  $NDVI_{AusE-clim}$  for 1982-2000 and  $NDVI_{MCD43A4}$  for 2000-2022,  
using a similar sampling approach as used for harmonisation only in this instance two models are built,  
205 a 'desert' model and 'non-desert' model. The non-desert model covers the same region as the high and  
low WCF models previously described (the inclusion of WCF in the features reduces the need to define  
a low and high WCF modelling region). GBM models were then fit using all the features previously



listed for the ‘clim’ model, plus de-seasonalised CO<sub>2</sub> concentration and annual WCF. Otherwise, the modelling framework was the same as the harmonisation approach. The synthetic NDVI datasets (NDVI<sub>SYN</sub>) are used to gap fill the NDVI<sub>AusE-clim</sub> record from January 1982 to February 2000. The final gap-filled, calibrated, and harmonised NDVI<sub>AusE-clim</sub> dataset is joined with NDVI<sub>MCD43A4</sub>. Only the NDVI<sub>AusE-clim</sub> dataset is gap filled, the NDVI<sub>AusE-noclim</sub> dataset is simply joined with the NDVI<sub>MCD43A4</sub> record. This ensures the ‘noclim’ dataset does not contain any climate information in the reconstructed time series.

## 215 2.4 Trends in peak-of-season phenology

Annual, per-pixel NDVI land surface phenology statistics were extracted using the “xr\_phenology” Python function from the “dea-tools” package (Krause et al., 2021). This analysis focused on two metrics, the NDVI value at the peak of the season (vPOS), and the day-of-year the peak occurs (POS). The input time-series was the gap-filled ‘clim’ dataset, and the time-series was first linearly up-sampled from monthly to two-week intervals to increase the temporal resolution of the datasets before the time-series was smoothed using a Savitsky-Golay filter with a window length of 11 and a polynomial order of three. Though we report day-of-year as the unit for POS, the actual POS could have occurred anytime withing a given bi-monthly time step, so DOY values should be considered an approximation.

To avoid applying phenology trend analysis on regions that do not experience regular seasonal variation, we created a mask that removes regions identified as ‘non-seasonal’ using the definitions and methods defined by Moore et al. (2016). Broadly, the mask is created using three inputs: the standard deviation in NDVI anomalies, long-term mean NDVI, and the standard deviation in the mean seasonal cycle. These three inputs are used to identify regions that experience either low seasonal variability and low NDVI, or low seasonal variability and high interannual variability, which largely coincide with the desert bioclimatic region.

Per-pixel linear trends in these phenology metrics were extracted using the Theil-Sen robust regression approach, and significance was determined using a Mann Kendall test (significance defined  $\alpha = 0.05$ ). Trends summarised over bioclimatic regions were extracted by first calculating per-pixel robust



235 regression on the phenology statistics, and then summarising the trends within a bioclimatic region with kernel density estimation (KDE) plots.

### 3 Results

#### 3.1 Quality of existing datasets.

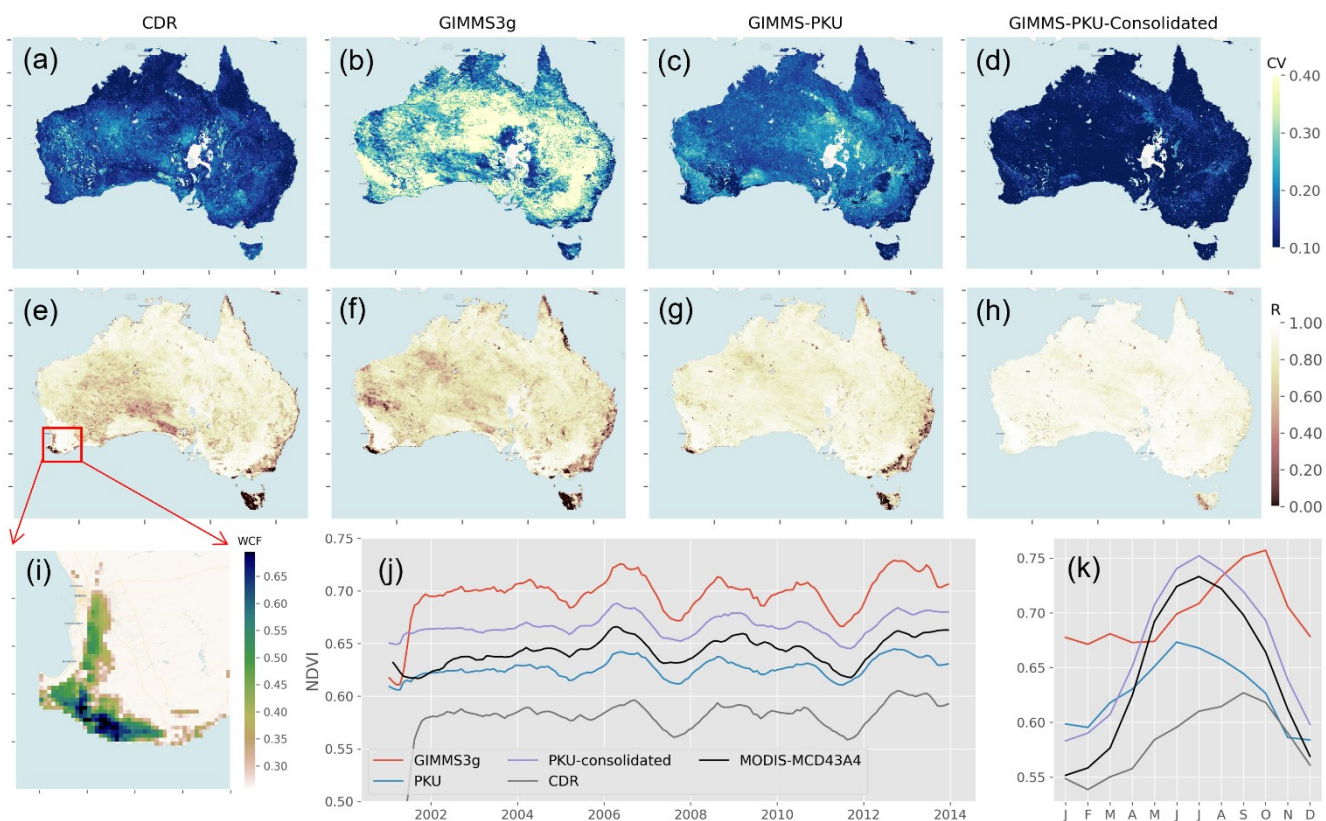
The quality of the  $NDVI_{AVHRR}$  products were compared against  $NDVI_{MCD43A4}$  for the overlapping years 2000-2013. All datasets except  $NDVI_{PKU-consolidated}$  perform poorly over regions with perennially high  
240 vegetation cover including wet coastal and highland forest ecosystems, where correlations between  $NDVI_{AVHRR}$  and  $NDVI_{MCD43A4}$  are close to zero in some regions (Figure 2e-g).  $NDVI_{CDR}$  and  $NDVI_{GIMMS3g}$  also poorly represent the desert region with  $R^2$  scores are as low as  $\sim 0.4 - 0.5$ .  $NDVI_{PKU-consolidated}$  correlates very well with  $NDVI_{MCD43A4}$  over most of the continent, with the exception of western Tasmania (Figure 2h). Coefficients of variation are also high for the  $NDVI_{GIMMS3g}$  and  
245  $NDVI_{PKU}$  datasets across much of the continent (Figure 2b-c) with average values of 0.33 and 0.18, respectively (Figure 2b-c).

To demonstrate how the discrepancies over densely vegetated ecosystems would impact, Figure 2j-k presents a zonal timeseries of the woodlands of south-west Western Australia. These woodlands have been identified as a region of high endemic biodiversity (Myers et al., 2000; Hopper and Gioia,  
250 2004), are vulnerable to the effects of long-term climate change and are undergoing long-term shifts in climate (O'donnell et al., 2012; Hughes, 2011; Pitman et al., 2004; Hope et al., 2006). The MODIS-era interannual variability of these forests through a rolling twelve-month mean timeseries (Figure 2j) and reveal that all products capture interannual variability of the MODIS era reasonably well, though the long-term mean NDVI value varies substantially between products. The mean seasonal cycle, shown in  
255 Figure 2(k) (calculated from 2001-2013), reveals that the seasonal cycle of the forest ecosystem is very poorly represented in three of the four products, while  $NDVI_{PKU-consolidated}$  tracks the overall shape of the seasonal cycle well, but predicts a longer growing season. Discrepancies in seasonality are further highlighted in the per-pixel climatological 'month-of-maximum' NDVI plots (Figure A2 in the appendix). Estimates of even this relatively straightforward metric of seasonality are greatly impacted



260 by the choice of dataset, with desert, savanna, and forested regions varying substantially between  
datasets, sometimes by as much as several months in the case of forested regions in Tasmania and  
south-east Australia. The Australian-wide seasonal cycles likewise reveal substantial variation between  
products (Figure A2g).

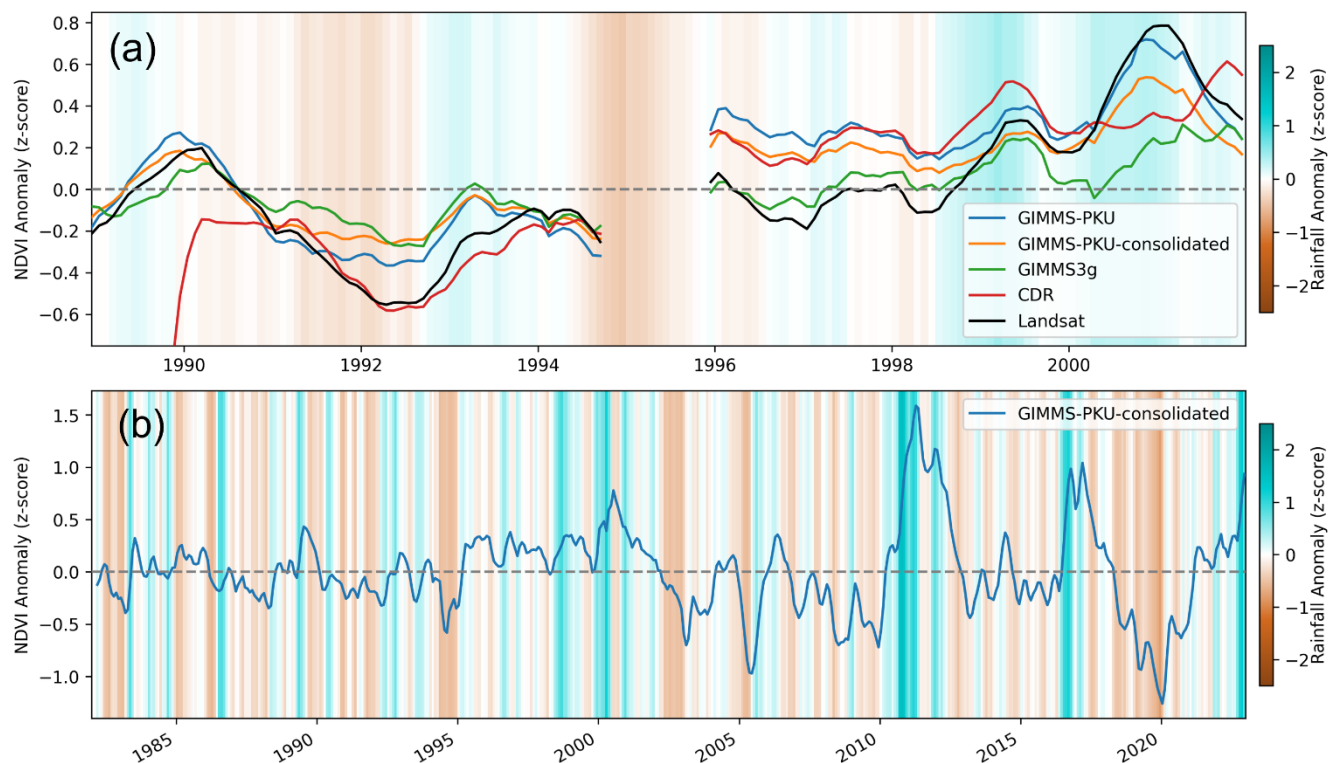
To assess the quality of  $NDVI_{AVHRR}$  products in the pre-MODIS era, Figure 3a compares the  
265 twelve-month rolling mean standardised anomalies of  $NDVI_{Landsat}$  in the 1988-2000 period (based on a  
1988-2012 climatology) with  $NDVI_{AVHRR}$  anomalies. No product accurately tracks  $NDVI_{Landsat}$   
anomalies across the whole 1988-2000 period. Only the  $NDVI_{PKU}$  product captures the amplitude of  
the La Niña driven positive anomaly of NDVI in 2000 (but recall that  $NDVI_{PKU}$  is trained on the  
 $NDVI_{Landsat}$  archive). In Australia, vegetation growth across the continent is strongly water-limited  
270 (Peters et al., 2021; Poulter et al., 2014; Broich et al., 2014), so it is our expectation that similarly





275 **Figure 2: Comparisons between  $NDVI_{MCD43A4}$  and four versions of  $NDVI_{AVHRR}$ . a-d) The coefficient of variation (CV) between  $NDVI_{MCD43A4}$  and  $NDVI_{AVHRR}$  where RMSE is divided by the 2001-2013 mean of  $NDVI_{MCD43A4}$ . e-h) Pearson correlation ( $r$ ) between  $NDVI_{MCD43A4}$  and  $NDVI_{AVHRR}$ . i) Woody cover fraction (WCF) of the forests in south-west Western Australia indicating the location of the zonal time-series of (j) and (k). j) Twelve-month rolling mean NDVI timeseries of the forests of south-west Western Australia. k) Mean seasonal cycle of the forests of south-west Western Australia calculated over the 2001-2013 period.**

280 large negative and positive rainfall anomalies should result in similar NDVI anomalies in the pre-MODIS and MODIS eras. Taking the best of the products identified in the comparison with  $NDVI_{MODIS}$ , Figure 3b shows the three-month rolling mean standardised anomalies of  $NDVI_{PKU-consolidated}$  from 1982-2022. In the MODIS era,  $NDVI_{PKU-consolidated}$  responds strongly to anomalies in rainfall (background shading shows the continental average standardised rainfall anomalies), while in the pre-MODIS era significant droughts (e.g., 1982-83) and widespread rainfall events (e.g., 2000) produce comparatively little effect in NDVI, suggesting a lack of rainfall-driven variability over Australia in the pre-MODIS era. Thus, we argue that no current  $NDVI_{AVHRR}$  product currently satisfies our criteria of a product that both agrees well with  $NDVI_{MCD43A4}$  while also producing satisfactory results in the pre-MODIS era.



290

**Figure 3:** a) Twelve-month rolling mean standardised anomalies of Landsat, CDR, GIMMS3g, GIMMS-PKU, and GIMMS-PKU-consolidated NDVI, based on a common 1988-2012 climatology. Background shading represents twelve-month rolling mean standardised rainfall anomalies. All datasets, besides rainfall, have matching data gaps. b) Three-month rolling mean standardised anomalies of the NDVI<sub>PKU-consolidated</sub> product (1982-2022 climatology). Background shading represents three-month rolling mean standardised rainfall anomalies.

295

### 3.2 Calibration and harmonisation performance

Independent validation statistics for all six model varieties ('clim' and 'noclim'; desert, high and low WCF) reveal a high degree of agreement in all model types with  $R^2 \geq 0.91$  for the 'clim' models, and MAE  $\leq 0.028$ . The 'clim' model types (Figure 4a-c) tended to have errors  $\sim 15\%$  smaller than their 'noclim' counterparts (Figure 4d-f). SHAP feature importance plots indicate NDVI<sub>CDR</sub> as the most important variable (Figure A3), but in the high WCF regions the relative importance of NDVI<sub>CDR</sub> diminished and NDVI<sub>MCD43A4</sub> summary statistics, solar radiation, and cumulative rainfall substantially impacting predictions (Figure A3b,c). Orbital parameters (SZEN, TOD) tended to have little effect on predictions regardless of model type.

305

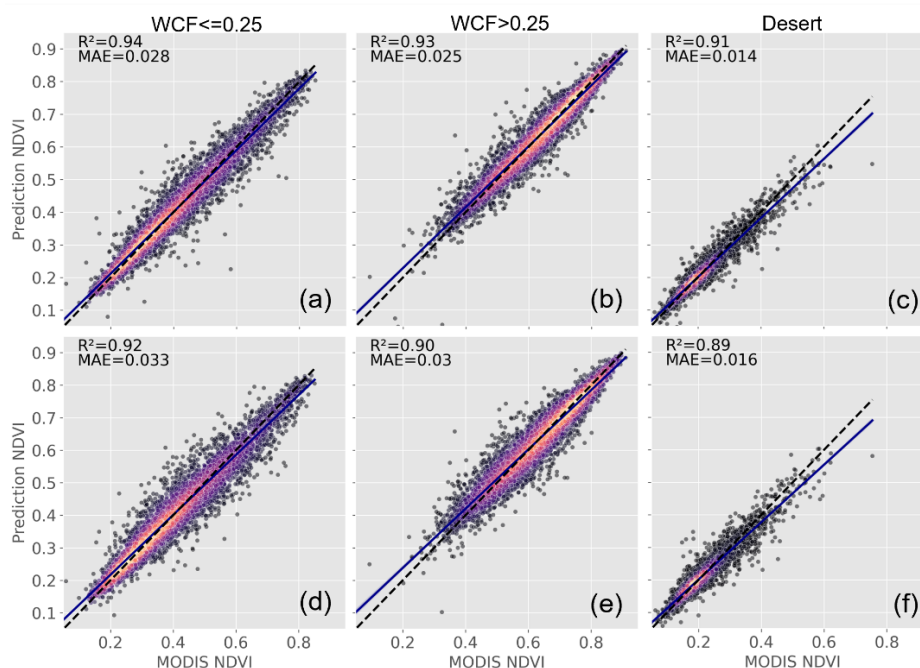
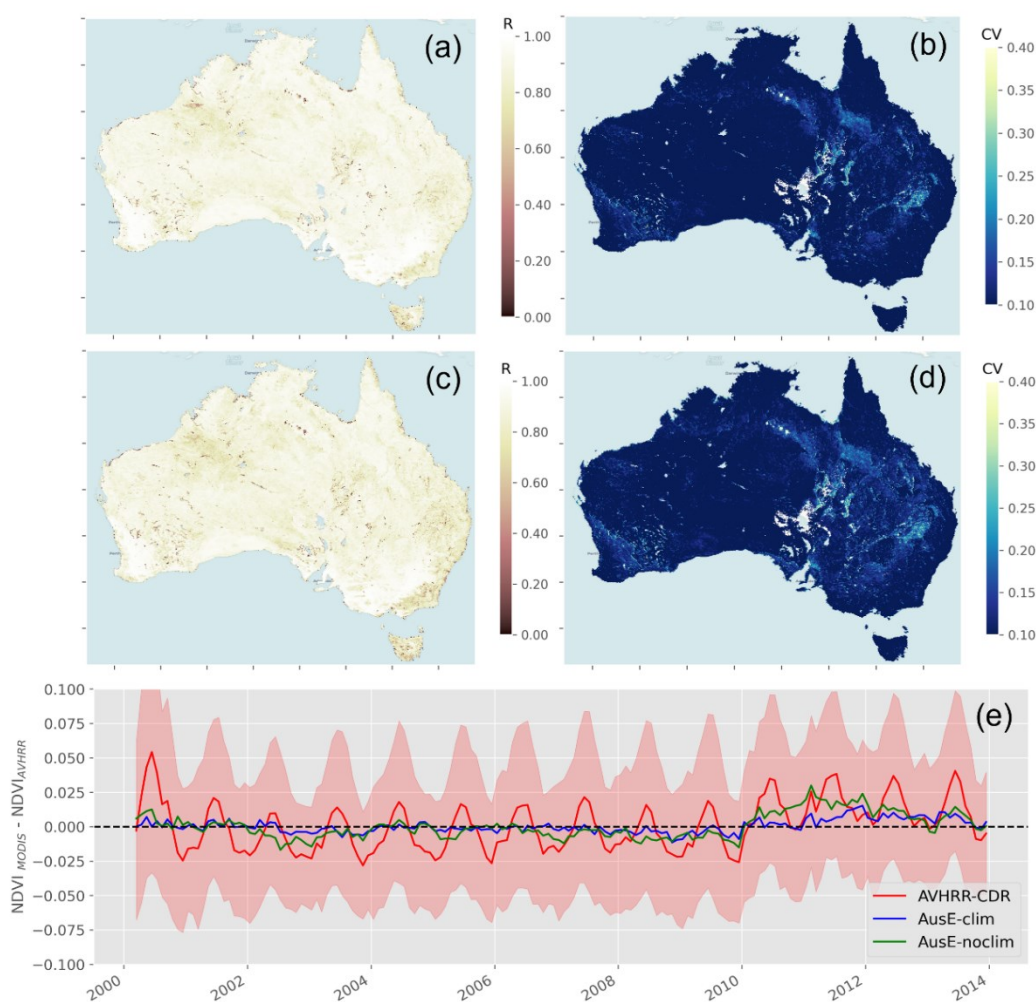


**Figure 4: Validation scatter plots for the calibration and harmonisation between  $NDVI_{CDR}$  and  $NDVI_{MCD43A4}$ . (a-c) show the results for the ‘clim’ model. (d-f) shows the same but for the ‘noclim’ model type.**

Per pixel agreements between  $NDVI_{AusE}$  and  $NDVI_{MCD43A4}$  for both the ‘clim’ and ‘noclim’  
310 model types reveal a very high degree of correlation across the continent (note that pixels with a long-term average  $NDVI \leq 0.11$  are masked for this analysis). Correlations between  $NDVI_{MCD43A4}$  and  $NDVI_{AusE}$  in Australia’s forested ecosystems have been greatly improved, averaging  $R^2 = 0.90$  in the ‘clim’ model (average  $R^2$  in the CDR product is 0.58). Areas of lower correlation persist in places that experience ephemeral or periodic water inundation such as mangroves and inland lake systems.  
315 Relative error has been reduced universally across the continent, with a continental average CV of <10 % (figure 5b). Areas of greatest relative error occur in the channel country in Australia’s arid interior, and the irrigated regions of the northern Murray Darling Basin. The ‘noclim’ model performs similarly, though correlations and relative error are universally worse than the ‘clim’ model (figure 5c-d). Residual NDVI values after subtracting  $NDVI_{AVHRR}$  from  $NDVI_{MCD43A4}$  before and after the calibration  
320 and harmonisation show the GBM model has entirely removed the residual seasonal signal present in the CDR product, resulting in residuals that closely track the zero line. Some small bias remains in the 2011-2012 period (especially for the ‘noclim’ model) when anomalously large rainfall related to a



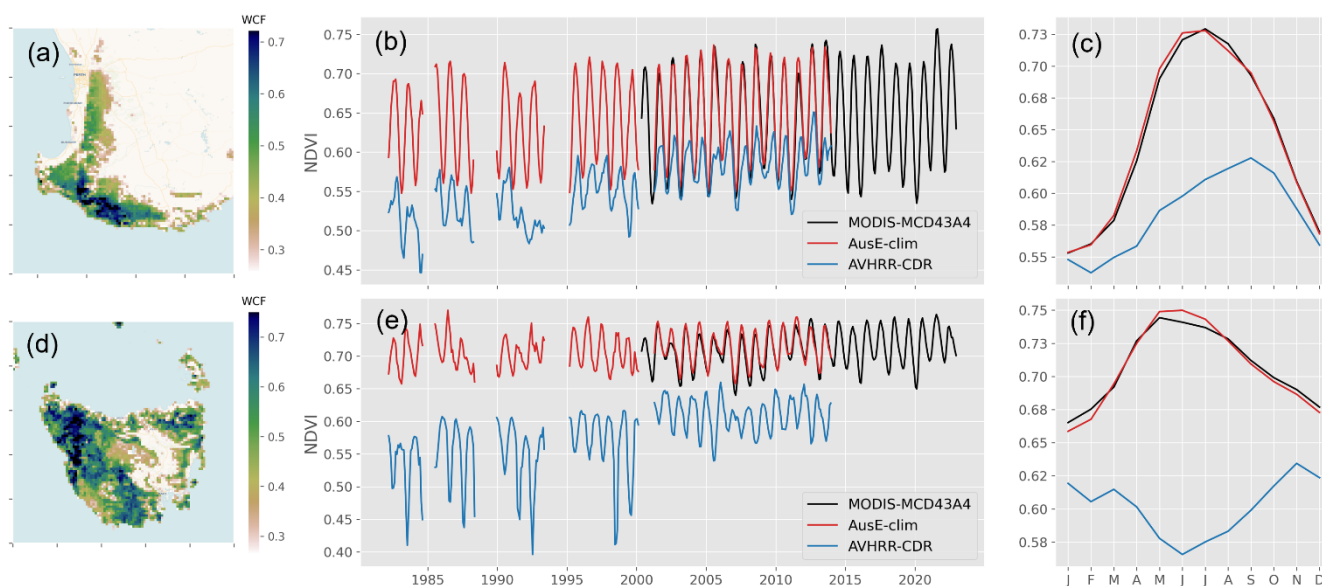
major La Nina event resulted in anomalous greening in the savanna and desert biomes. This is further illustrated in figure A4 where NDVI timeseries before and after the adjustment have been summarised over six bioclimatic regions (extents in Figure 1b). Differences in the Australia-wide time-series between  $NDVI_{MCD43A4}$  and  $NDVI_{AusE}$  are largely attributable to  $NDVI_{AusE}$  underestimating peak NDVI during 2011-2012 in the desert and savanna biomes (figure A4f-g).



330 **Figure 5:** Results of the calibration and harmonization between  $NDVI_{CDR}$  and  $NDVI_{MCD43A4}$ . a) shows the per pixel Pearson correlation, between  $NDVI_{MCD43A4}$  and 'clim'  $NDVI_{AusE}$ . b) shows the same as (a) but for the coefficient of variation. c-d) the same as (a-b) but for the 'noclim' model type. e) The residual NDVI value when subtracting  $NDVI_{AVHRR}$  from  $NDVI_{MCD43A4}$  before and after the calibration and harmonization. Residuals are calculated per pixel and then averaged over Australia. Shading indicates the standard deviation in residuals across the continent for the  $NDVI_{CDR}$  product.



335 Improvements in the alignment between  $NDVI_{AVHRR}$  and  $NDVI_{MCD43A4}$  from this regional  
calibration and harmonisation are further demonstrated in Figure 6 where timeseries are summarised  
over two challenging forest ecosystems in southwest Western Australia and Tasmania. Mean seasonal  
cycles between the two NDVI datasets are now in very close agreement (figure 6c, f) and the  $NDVI_{AusE}$   
time-series from 1982-2000 ('clim' is shown) can effectively integrate with the  $NDVI_{MCD43A4}$  time-  
340 series without introducing major discontinuities (figure 6b, e).



345 **Figure 6: Results before and after the calibration and harmonisation of  $NDVI_{CDR}$  for two example high woody canopy cover regions previously identified as having the worst agreement with  $NDVI_{MCD43A4}$ . b-c) Three-month rolling mean 1982-2022 NDVI time series, and the mean seasonal cycle (averaged over the 2001-2013 period), respectively, for the forests of south-west Western Australia. e-f) Same as (b-c) but for Tasmanian forests. Time series are the spatial average of the regions to their left.**

### 3.2 Gap-filling with Synthetic NDVI

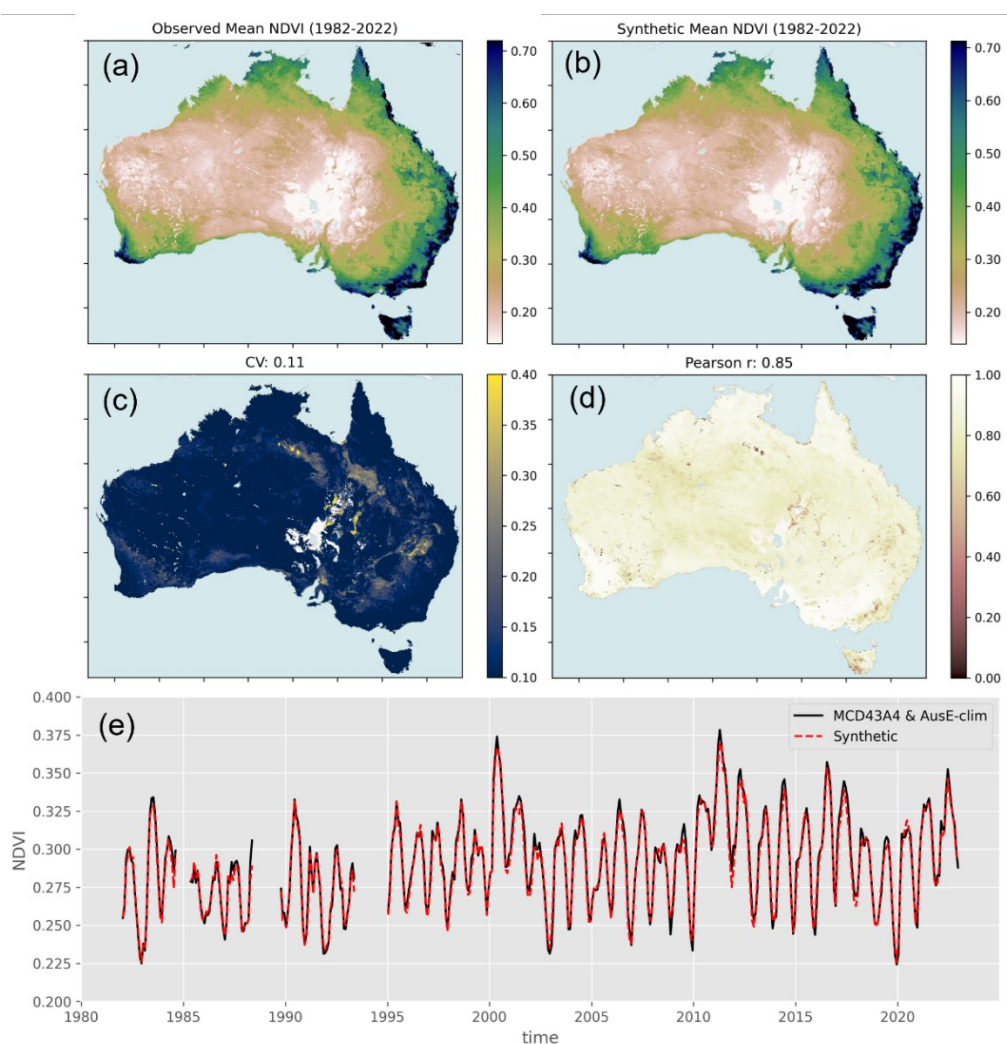
The  $NDVI_{SYN}$  dataset record agrees exceptionally well with the joined  $NDVI_{AusE-clim}$  and  $NDVI_{MCD43A4}$  series when aggregated across Australia (Figure 7e). At the pixel level, the long-term mean NDVI of  
350 both datasets is virtually identical (Figure 7a-b). Per-pixel Pearson correlation averages 0.85 across the continent (figure 7d). Areas of poorer correlation occur in western Tasmania, the highlands forests of south-east Australia – all areas that experience seasonal snow fall – and regions of either anthropogenic water application (irrigation) or ephemeral, delayed water inundation (inland rivers in the arid interior).



355 Mean relative error was also low, averaging 11 %, but with hotspots of greater error again occurring in the regions where water inundation is not dependent on direct rainfall (Figure 7c).

We present validation scatter plots and feature importance plots for the desert and non-desert GBM models in the appendix (figure A5). In the non-desert region, three-month cumulative rainfall and VPD are the key climate drivers of predictions, while in the desert region, six-month cumulative rainfall, VPD, and incoming solar radiation are the key climate drivers.

360

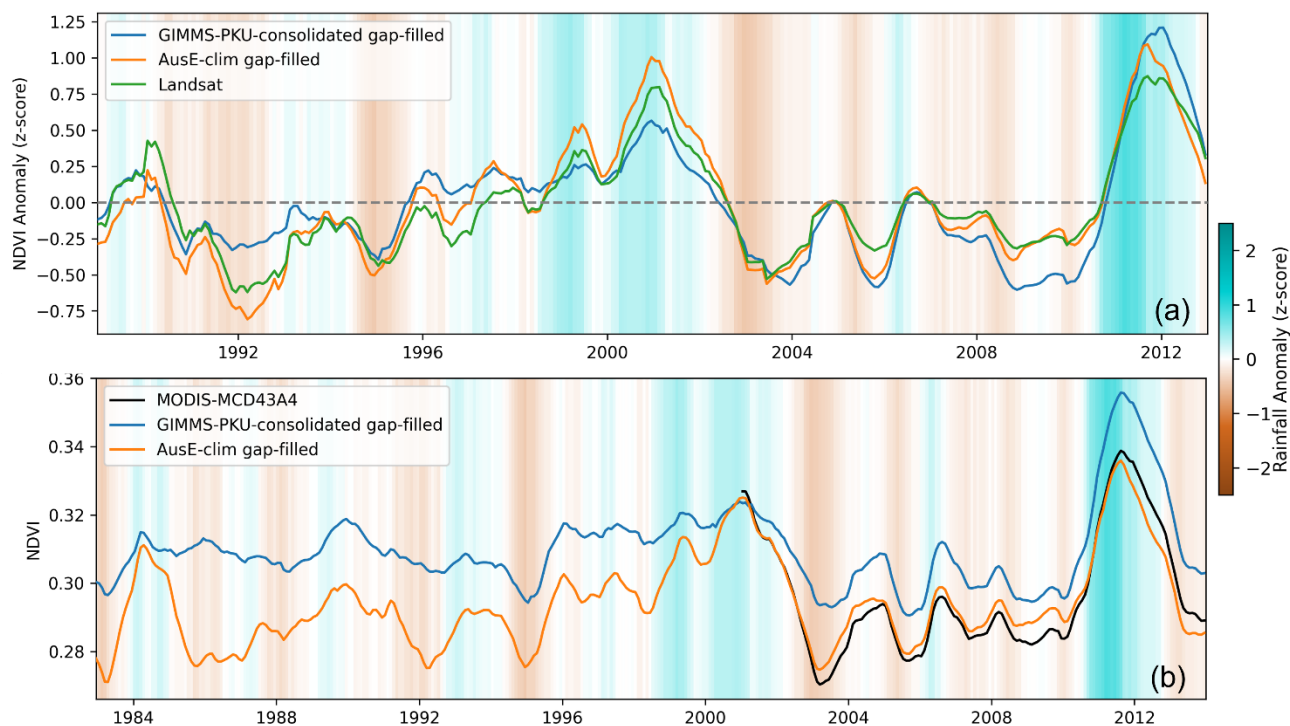


365 **Figure 7: Evaluation of the synthetic NDVI built to gap-fill the  $NDVI_{AusE-clim}$  record** a-b) show the observed and synthetic long-term mean NDVI, respectively. c) per pixel coefficient of variation (CV) between observed NDVI and synthetic NDVI. d) Same as (c) but Pearson correlation. e) Continentally averaged observed and synthetic NDVI timeseries, where data gaps have been matched.



### 3.3 Comparison with Landsat and MODIS NDVI annual time series

Comparing the calibrated, harmonised, and gap-filled  $\text{NDVI}_{\text{AusE-clim}}$  dataset with rolling annual mean  $\text{NDVI}_{\text{Landsat}}$  anomalies reveals a good level of agreement in both the timing and magnitude of inter-annual variability throughout the 1988-2012 period (figure 8a).  $\text{NDVI}_{\text{PKU-consolidated}}$  is also shown for comparison and gaps in the  $\text{NDVI}_{\text{PKU-consolidated}}$  dataset have been filled using the same synthetic data and procedure as  $\text{NDVI}_{\text{AusE-clim}}$  to facilitate a more straightforward comparison and continuous time-series.  $\text{NDVI}_{\text{AusE-clim}}$  consistently outperforms  $\text{NDVI}_{\text{PKU-consolidated}}$ . A comparison with  $\text{NDVI}_{\text{MCD43A4}}$  is shown in Figure 8b where all three time series are plotted as a simple rolling annual mean.  $\text{NDVI}_{\text{AusE-clim}}$  aligns well with  $\text{NDVI}_{\text{MCD43A4}}$  at the annual timescale and records greater rainfall driven inter-annual variability in the pre-MODIS era. The historic 1982-2000 archive can clearly join with the  $\text{NDVI}_{\text{MCD43A4}}$  series without introducing major discontinuities.



380 **Figure 8:** a) Twelve-month rolling mean standardised NDVI anomalies of the gap-filled  $\text{NDVI}_{\text{AusE-clim}}$  plotted alongside Landsat anomalies and  $\text{NDVI}_{\text{PKU-consolidated}}$  anomalies. Gaps in the  $\text{NDVI}_{\text{PKU-consolidated}}$  dataset have been filled using the same synthetic data and procedure as  $\text{NDVI}_{\text{AusE-clim}}$ . All datasets are matched to Landsat data gaps. b) Twelve-month rolling mean NDVI time-series of the gap-filled, calibrated, and harmonised  $\text{NDVI}_{\text{AusE-clim}}$  over Australia from 1982-2013, plotted alongside  $\text{NDVI}_{\text{PKU-consolidated}}$  (gap-filled in the same manner as (a)), and  $\text{NDVI}_{\text{MCD43A4}}$ . Background shading on both a) and b) represents twelve-month rolling mean



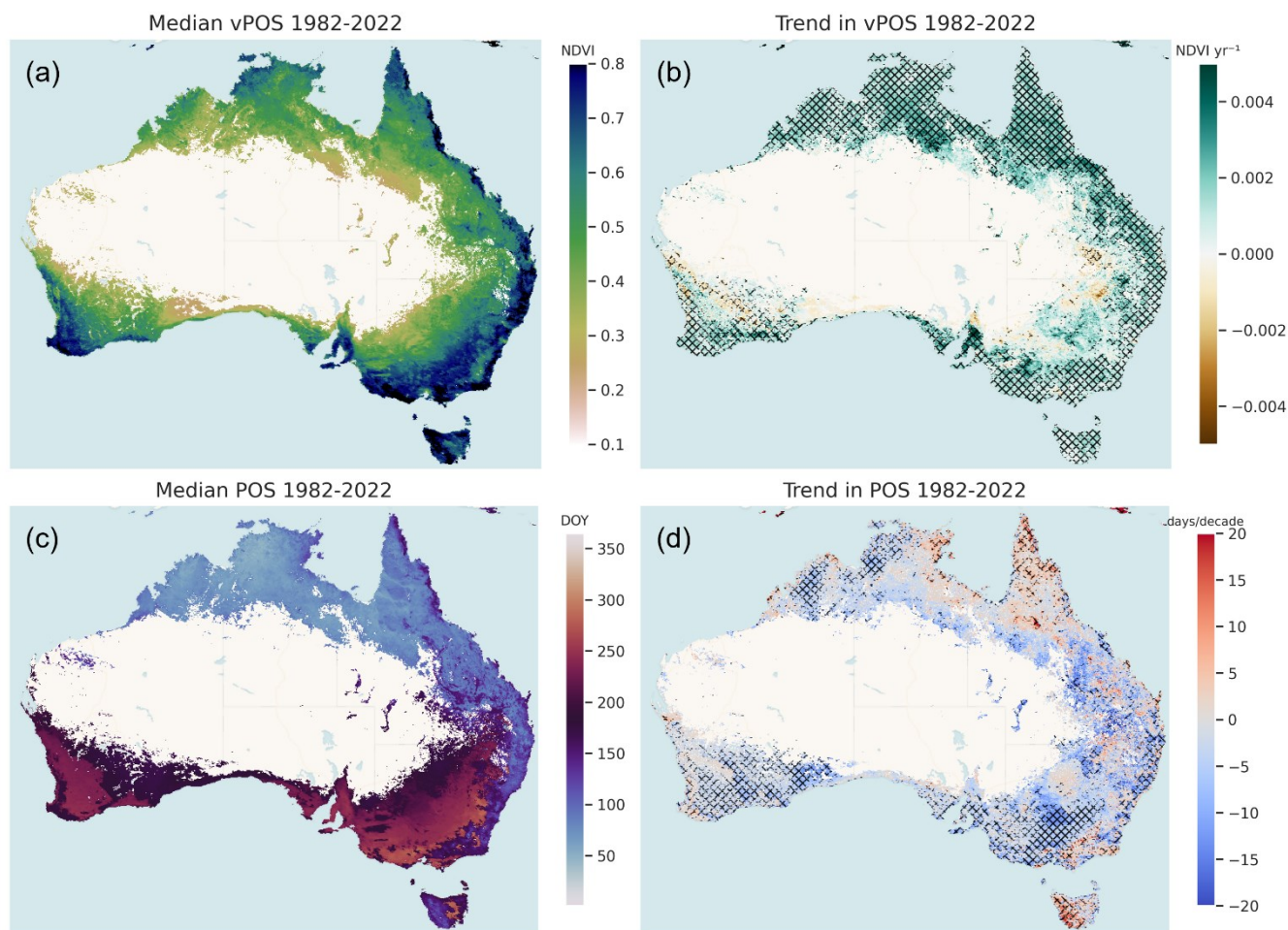
standardised rainfall anomalies across Australia where (a) is based on 1988-2012 climatology and (b) is based on a 1982-2012 climatology.

### 385 3.4 Trends in peak-of-season phenology

Per-pixel trends in vPOS, POS and the 40-year median values for these statistics are shown in Figure 9. Trends in vPOS are almost universally positive across the continent (hatching indicates a significant trend), with the exceptions of inland northern Murray-Darling Basin, the eastern periphery of the wheat belt in Western Australia, and the region north of Adelaide (figure 9b). Positive trends observed in the  
390 major agricultural region of the Murray-Darling Basin and the northern half of the West Australian wheat belt and are non-significant. Distributions of trends in vPOS, stratified by bioclimatic region, reveal the highest median trends are recorded in the tropics and savanna regions at 0.0013 and 0.0014 NDVI yr<sup>-1</sup>, respectively (figure A6a-e). The Mediterranean region has the lowest median trend at 0.0009 NDVI yr<sup>-1</sup>.

395 Trends in the day-of-year that peak NDVI occurs (POS) are negative across much of the continent, suggesting there is a general tendency for NDVI to peak earlier in the year across Australia. Significant negative trends occur in the agricultural zones of the Mediterranean bioclimatic region, the greater western woodlands that border the eastern margin of the WA wheatbelt, the western half of the Nullabor plain, parts of the Riverina agricultural region of south-western New South Wales and  
400 extending into Victoria, and western parts of the northern tropical savanna. These significant negative trends are reflected in the POS trend distributions in figure A6f-j where the median trend in the warm temperate and Mediterranean regions are highest at 3.4 and 2.3 days per decade, respectively. Significant positive trends (peak NDVI occurring later in the year) are observed in tropical northern Queensland and western Tasmania and can be as high as 5-10 days per decade.

405



410 **Figure 9:** a) The median annual peak NDVI value (vPOS) from 1982-2022. b) Theil-Sen robust regression trends in vPOS. c) Median day-of-year that peak NDVI occurs (POS), 1982-2022. d) Theil-Sen robust regression trends in POS. Hatching on trend plots indicates significance at  $\alpha=0.05$  using a Man-Kendall test. All plots are derived from the gap-filled ‘clim’ NDVI<sub>AusE</sub> dataset. Non-seasonal areas have been masked using the method described in section 2.4.

## 4 Discussion

We expected to identify differences between NDVI<sub>AVHRR</sub> datasets given their different pre-processing and atmospheric corrections methods, different spatial resolutions, and differing temporal compositing techniques. Likewise, lower correlations in the densely vegetated regions were also expected due to the total variance in evergreen forests being smaller than for seasonal vegetation (grassland, croplands), and therefore, assuming a similar unexplained variance (noise), correlations should necessarily be weaker.

415



Nonetheless, we were surprised by the poor performance of global NDVI<sub>AVHRR</sub> products in representing the seasonal dynamics of Australia's densely vegetated regions. Why this is the case deserves a greater focus of study than we devote here but is likely related to some combination of the presence/absence of  
420 BRDF and water-vapour corrections, varying contamination by clouds, any gap-filling procedures applied, and the saturation effect of NDVI in higher canopy cover regions such as forests. Regardless of the reasons why, the intercomparison between NDVI<sub>AVHRR</sub> products highlights that global datasets, while often performing adequately when statistics are aggregated at the global or continental scale, can mask disparities that are important at the regional to local scale (Meyer and Pebesma, 2022). We  
425 advocate closely examining regional and local contexts to assess how suitable a given NDVI dataset is for a particular use case. For example, in Australia seasonal cycles in NDVI<sub>CDR</sub> are highly suspect and thus should not be relied upon for phenology studies. However, unlike GIMMS3g, NDVI<sub>CDR</sub> has a comparatively low relative error when compared with MODIS and displays reasonable inter-annual variability so would likely be more suited to long-term studies of agricultural drought frequency or the  
430 impacts of CO<sub>2</sub> fertilisation on maximum canopy cover (assuming sensor transitions are filtered). In Australia, the best use of NDVI<sub>PKU-consolidated</sub> is likely the reverse, its representation of seasonal cycles is good, while IAV is subdued in the pre-MODIS era. In general, we urge caution in using existing global NDVI<sub>AVHRR</sub> products for studying vegetation trends and seasonality in Australia. AusENDVI shows significant improvement over existing global datasets in this respect. The improved correspondence in  
435 seasonal cycles between NDVI<sub>AusE</sub> and NDVI<sub>MCD43A4</sub> provides evidence that AusENDVI is more suitable for exploring longer-term changes to Australia's vegetation phenology. The addition of climate features to the calibration and harmonisation also appears to have improved the representation of long-term interannual variability, thus AusENDVI-clim should likewise offer a better basis for studying the shifting frequency of extreme climate events and their impact on the terrestrial biosphere.

440 The creation of a synthetic NDVI using only climate, CO<sub>2</sub> concentration, and woody cover fraction as predictors revealed a high degree of predictability in NDVI over much of Australia. Regions of lower predictability were located where water supply is either from elsewhere or delayed (ephemeral inland rivers) or from irrigation. In the absence of features that could describe water supply without rainfall, NDVI patterns in these zones will continue to be difficult to estimate if direct satellite



445 observations are unavailable. Notwithstanding some spatial variability in per-pixel predictability, in  
general the high degree of agreement between observed and synthetic NDVI presents the prospect of  
extending the synthetic NDVI further back in time through the observational climate record, which in  
Australia is reliable throughout much of the 20<sup>th</sup> century. In land surface models, a dynamic phenology  
algorithm is an important sub-model which influences the overall carbon cycle, evapotranspiration, and  
450 energy balance of the model (Chen, 2022). The long-term record of synthetic NDVI developed here  
could, therefore, prove useful for validating the development of process-based phenology models for  
Australia's diverse range of vegetation and climate. Or, with empirically validated NDVI-LAI  
relationships, AusENDVI could be used as a phenology forcing during the pre-satellite era for the many  
LSMs that do not dynamically simulate LAI.

455 There are several sources of uncertainty in AusENDVI. Firstly, the climate and landscape  
features used are subject to their own uncertainties which will undoubtedly propagate into both the  
calibration and harmonisation, as well as the gap-filling with synthetic NDVI. For example, rainfall  
station observations in the arid interior of Australia are relatively sparse so errors in the spatial  
interpolation of rainfall are highly likely. Uncertainties in the NDVI<sub>CDR</sub> product are also likely to be  
460 transmitted to our dataset. Future work may include a greater treatment of uncertainty through ensemble  
modelling where climate features (e.g., different rainfall and solar radiation datasets), and model types  
used for fitting are iterated to generate an uncertainty envelope. We also aim to assess how well NDVI  
from the Visible Infrared Imaging Radiometer Suite (VIIRS) agrees with NDVI<sub>AusE</sub> and NDVI<sub>MCD43A4</sub>  
over Australia. Should there be a substantial discrepancy, the methods described here could be applied  
465 to VIIRS to create an ongoing, updated NDVI dataset for Australia than can continue to form the  
foundation for continental-scale studies of terrestrial ecosystem change. Irrespective, we argue our  
AusENDVI estimates are based on the best available data, while the gradient boosting models have  
gone through extensive cross-validation. Therefore, we contend that the resulting trends should be more  
accurate than any alternative NDVI dataset.

470 We identified advances in the timing of POS across much of Australia's land mass (though not  
all). Over the Mediterranean, warm temperate, and cool temperate bioclimatic regions the median peak  
phenology trends were -2 to -3 days/decade. Advances in plant maturity in the southern hemisphere



from field data are also reported by Chambers et al. (2013) where the mean rate of change in plant maturity was 14 days/decade, mostly from temperate regions (63 % of their data are from grape-vines).  
475 This rate of change is comparable to the per-pixel rates of change in POS that are seen in parts of the Mediterranean and warm temperate regions where it is not uncommon to see negative trends ranging from 10-15 days/decade (figure 9d). However, the magnitude of a trend is influenced by the length of the time series so comparisons with variable length field data is difficult and shorter records are more likely to report a larger rate (Chambers et al., 2013). Advances in the timing of POS could be due to a  
480 combination of climate drivers. In the northern hemisphere, warming has led to earlier peak greening (Huang et al., 2023; Liu et al., 2021; Park et al., 2019). Warming can accelerate metabolism, so where water is non-limiting, leaf development can be faster. However, temperature increases also increase vapour pressure deficits which decrease water-use efficiency and can reduce plant productivity, though this effect may be compensated for by enhanced CO<sub>2</sub> (Rifai et al., 2022; Dusenage et al., 2019). Changes  
485 in the timing of peak rainfall may also contribute to shifts in the timing of peak NDVI. The timing of peak climatological rainfall has shifted since 1960 (Figure A7a-c), and there is some coincidence between trends in POS and shifts in rainfall POS (e.g., advancement around Adelaide). The goal of this study is not to draw conclusions on the likely drivers of seasonality change in Australia, but to argue that our dataset provides a more reliable means for tackling these questions. Future work will delve into  
490 a greater suite of phenology metrics (e.g., start-of-season, end-of-season, growing season length (Xie et al., 2023)), and explore the drivers of phenological change.

The pervasive positive trends in vPOS are consistent with results elsewhere and are likely due to the impacts of CO<sub>2</sub> fertilisation, which allows a given amount of precipitation to sustain a greater maximum level of plant production over time (Donohue et al., 2009; Donohue et al., 2013; Rifai et al.,  
495 2022; Ukkola et al., 2016). Increases in the magnitude of Austral spring and summer rainfall in northern Australia are also likely to have contributed to the widespread increase in vPOS in tropical Australia (Figure A7d). It is also likely that improving agricultural practices has increased maximum NDVI in the rain-fed cropping regions, especially in South Australia and Victoria where positive vPOS trends are significant. Trends in maximum NDVI in the WA wheatbelt are also positive, but contrast with the fact



500 that WA has seen a widespread autumn drying trend (Figure A7d). We speculate that agricultural innovation here has counteracted a drying trend that would otherwise have reduced foliage cover.

## 5 Data and Code Availability

AusENDVI is openly available at <https://doi.org/10.5281/zenodo.10802704> (Burton, 2024) and consists of several datasets. Each dataset has a description in the attributes of the NetCDF file that defines its  
505 provenance. A short description of each dataset is provided below as an additional reference. All datasets are in "EPSG:4326" projection, have a spatial resolution of 0.05°, and monthly temporal resolution. A Jupyter notebook is also provided at the above link demonstrating how to load, plot, mask, reproject, and gap-fill AusENDVI datasets.

- 510 • *AusENDVI-clim\_1982\_2013*. Calibrated and harmonised NOAA's Climate Data Record AVHRR NDVI data from January 1982 to December 2013. This version of the dataset used climate data in the calibration and harmonisation process. The dataset has not been gap filled, and extra data has been filtered/removed beyond the typical QA filtering using methods described in this publication.
- 515 • *AusENDVI-noclim\_1982\_2013*. Calibrated and harmonised NOAA's Climate Data Record AVHRR NDVI data from January 1982 to December 2013. This version of the dataset did not use climate data in the calibration and harmonisation process. The dataset has not been gap filled, and extra data has been filtered/removed beyond the typical QA filtering using methods described in this publication.
- 520 • *AusENDVI-synthetic\_1982\_2022*. This dataset consists of synthetic NDVI data that was built by training a model on the joined 'AusENDVI-clim' and 'MODIS-MCD43A4 NDVI' timeseries using climate, woody-cover-fraction, and atmospheric CO<sub>2</sub> as predictors.
- *AusENDVI-clim\_gapfilled\_MCD43A4\_1982\_2022*. This dataset consists of calibrated and harmonised NOAA's Climate Data Record AVHRR NDVI data from January 1982 to February  
525 2000, joined with MODIS-MCD43A4 NDVI data from March 2000 to December 2022. This



version of the dataset used climate data in the calibration and harmonisation process. The dataset has been gap filled using AusENDVI-synthetic,

- *AusENDVI-noclim\_MCD43A4\_1982\_2022*. This dataset consists of calibrated and harmonised NOAA's Climate Data Record AVHRR NDVI data from January 1982 to February 2000, and MODIS-MCD43A4 NDVI data from Mar. 2000 to Dec. 2022. This version of the dataset did not use climate data in the calibration and harmonisation process. The dataset has not been gap filled.

The code to conduct all analysis described here is available on the open-source repository:

<https://github.com/cbur24/AusENDVI>

## 6 Conclusion

We calibrated and harmonised  $NDVI_{CDR}$  to  $NDVI_{MCD43A4}$  for Australia using a well cross-validated gradient-boosting ensemble decision tree method. We developed two versions of the datasets, one that utilises climate data in the feature set to achieve the best possible agreement between  $NDVI_{CDR}$  and  $NDVI_{MCD43A4}$  ('AusENDVI-clim'); and a second dataset that does not rely on climate data ('AusENDVI-noclim'). The resulting datasets have a spatial resolution of  $0.05^\circ$  and extend from 1982-2013 and showed strong correlation and low relative errors with respect to  $NDVI_{MCD43A4}$ . They also closely reproduced the seasonal cycles of  $NDVI_{MCD43A4}$  over Australia's densely vegetated regions and can provide the basis for studies on Australia's changing vegetation phenology and downstream impacts on terrestrial carbon and water cycles. Moreover, they also closely replicate the interannual variability in vegetation condition in the pre-MODIS era as indicated by Landsat NDVI anomalies. Additionally, we developed a reliable method for gap filling the AusENDVI record by creating a synthetic NDVI dataset using only climate,  $CO_2$  concentration, and woody cover fraction as predictors. The resulting dataset showed excellent agreement with the observations, providing confidence in its use for gap filling. Lastly, we provide a complete 41-year long dataset where gap filled AusENDVI from January 1982 to February 2000 is seamlessly joined with  $NDVI_{MCD43A4}$  from March 2000 to December 2022.



AusENDVI estimates are based on the best available data, and we contend it is highly suitable for studying the impact of global environmental change on Australia's terrestrial vegetation.

## 555 Appendix

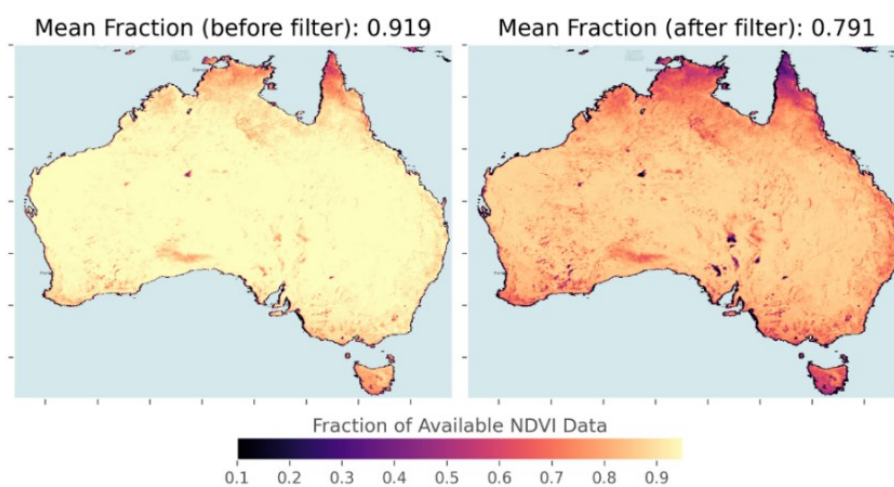
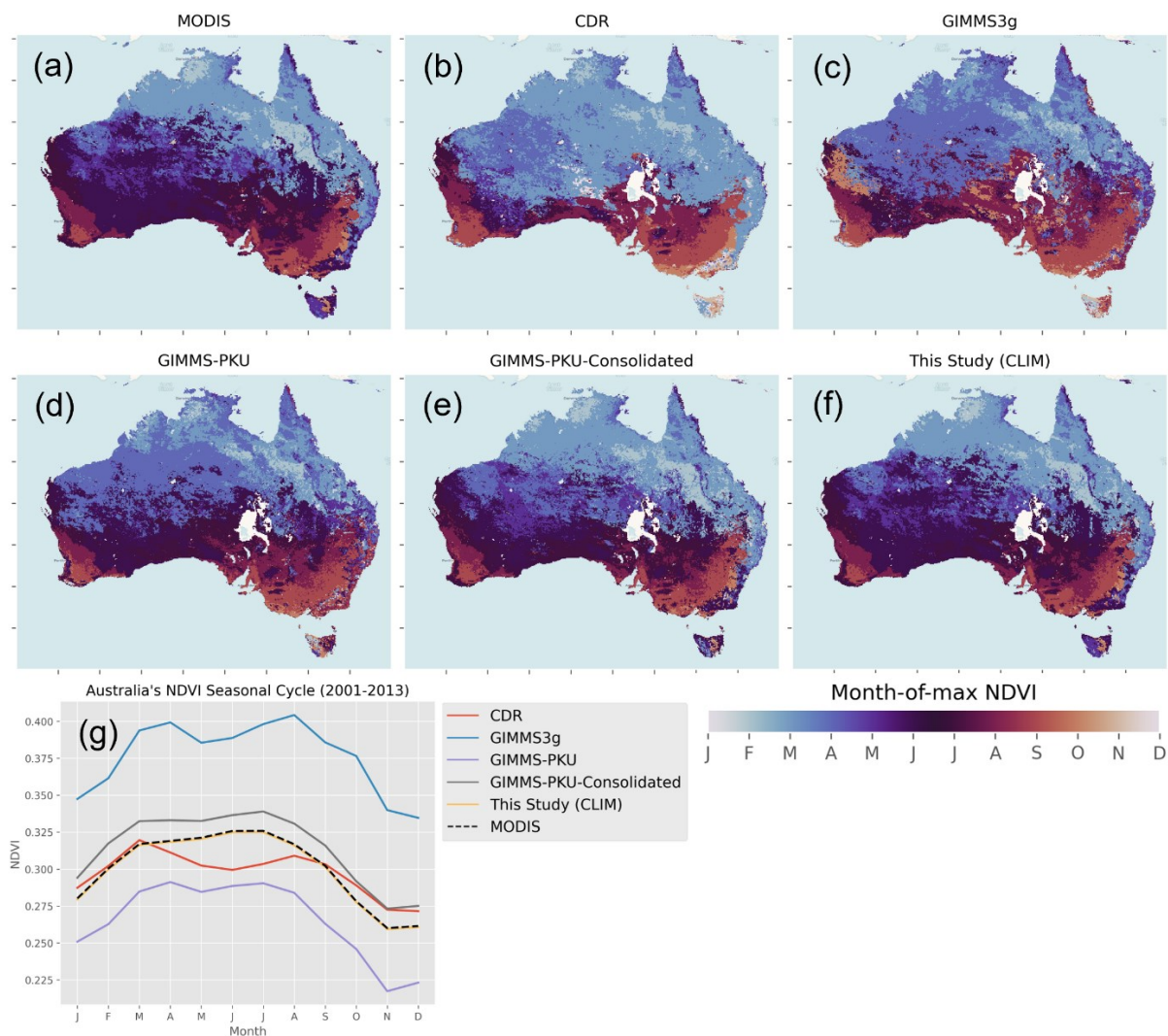
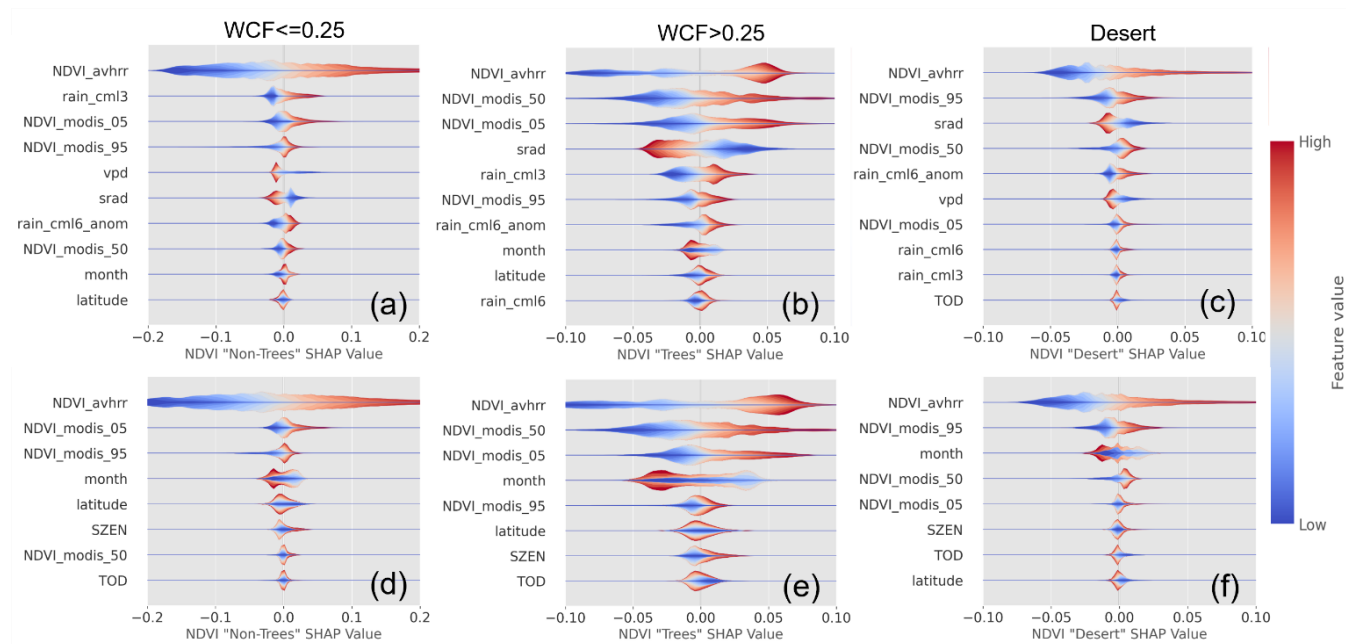


**Figure A1:** Available fractions of data before and after additional filtering of NDVI<sub>CDR</sub> data. A value of one means all monthly time-steps between 1982-2013 are preserved.



560 **Figure A2: a-f) Month that maximum NDVI occurs, averaged from 2001-2013, for all NDVI datasets included in the intercomparison between NDVI products, along with the AusENDVI-clim dataset of this study. g) The climatological mean seasonal cycle of NDVI summarised over Australia.**



565 **Figure A3: Feature importance plots for the calibration and harmonisation between  $NDVI_{CDR}$  and  $NDVI_{MCD43A4}$ . a-c) show the results for the 'clim' model. d-f) shows the same but for the 'noclim' model type.**

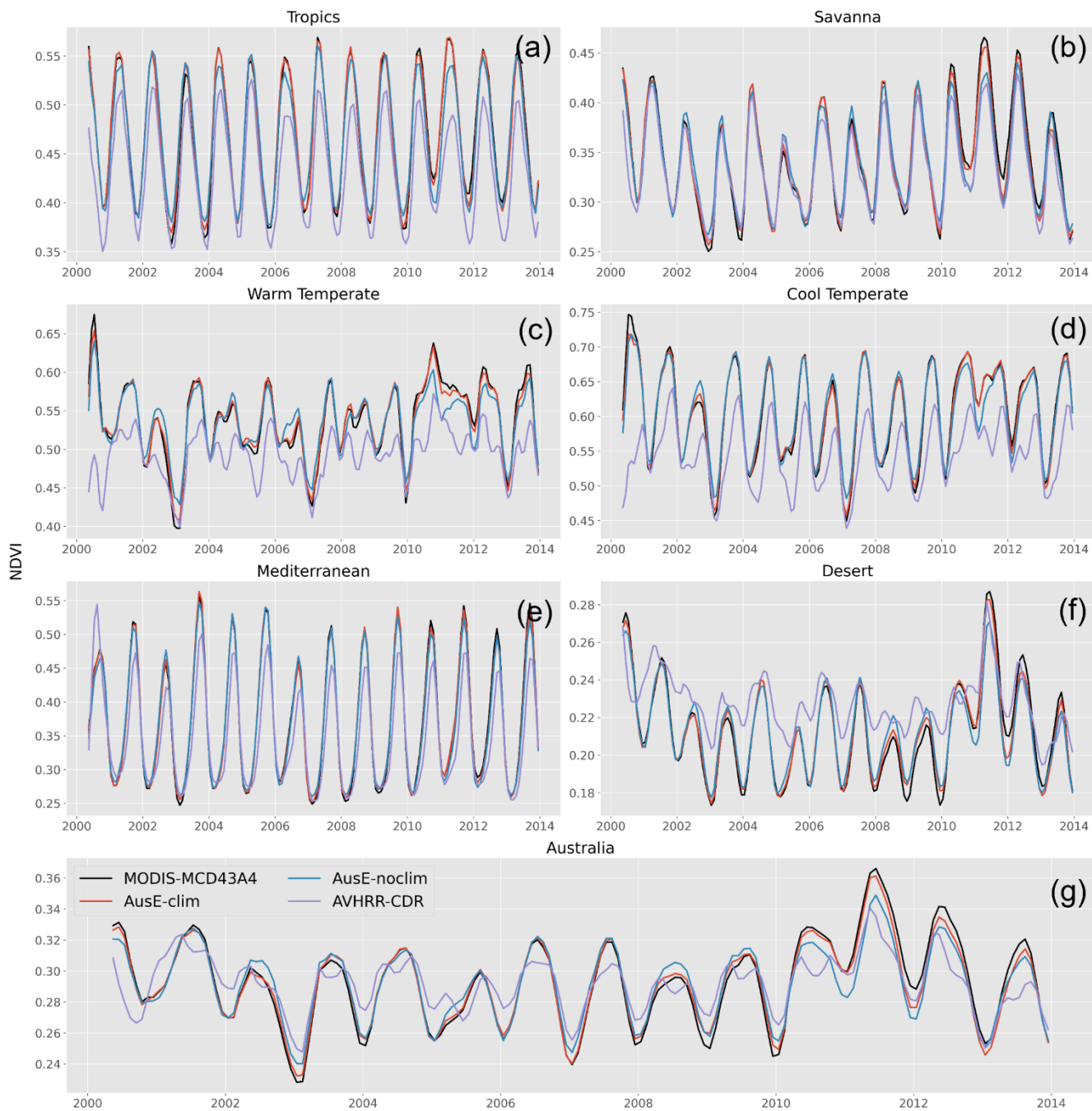
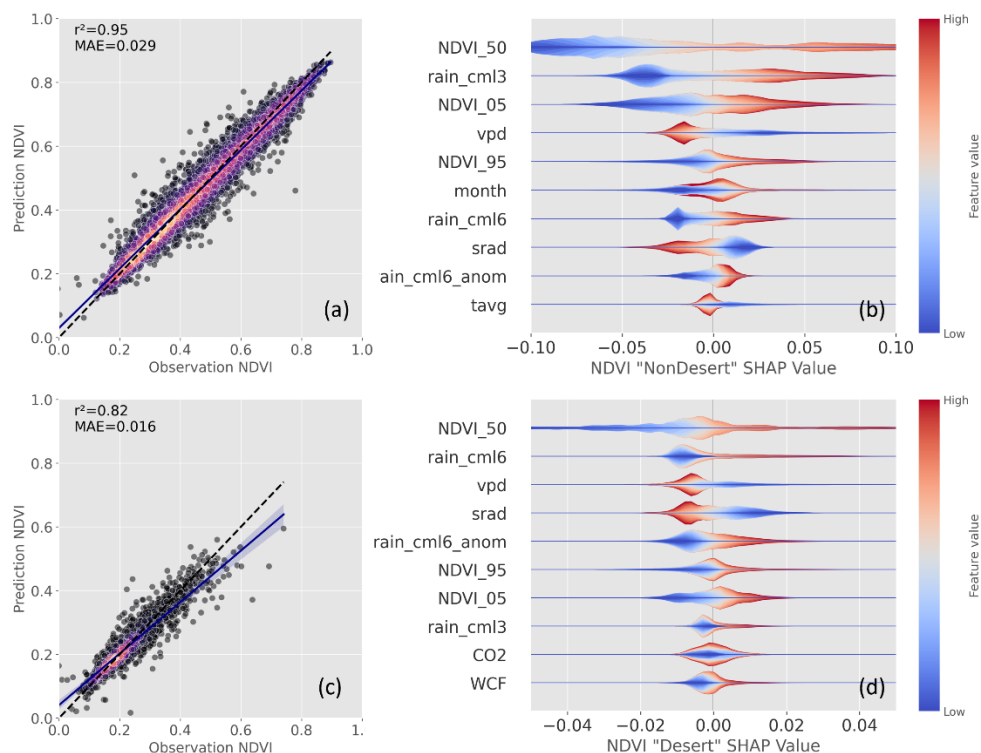
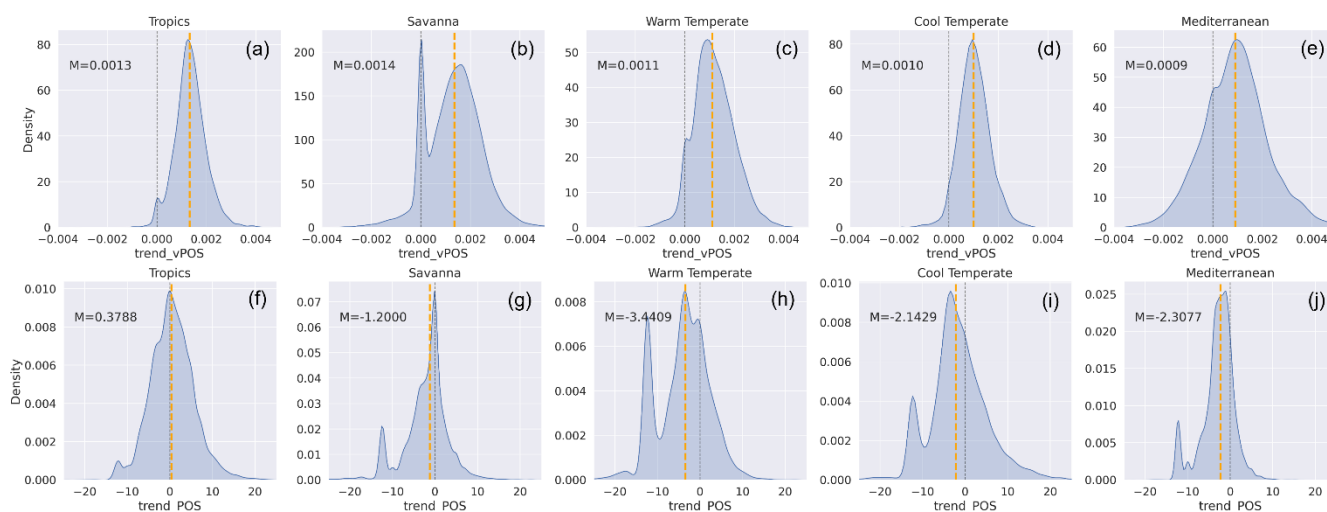


**Figure A4: Per bioregion (a-f) and Australia-wide (g) NDVI time-series before and after the calibration and harmonisation of  $NDVI_{CDR}$ . Bioregions are defined in Figure 1b. Time series have been smoothed with a three-month rolling mean.**

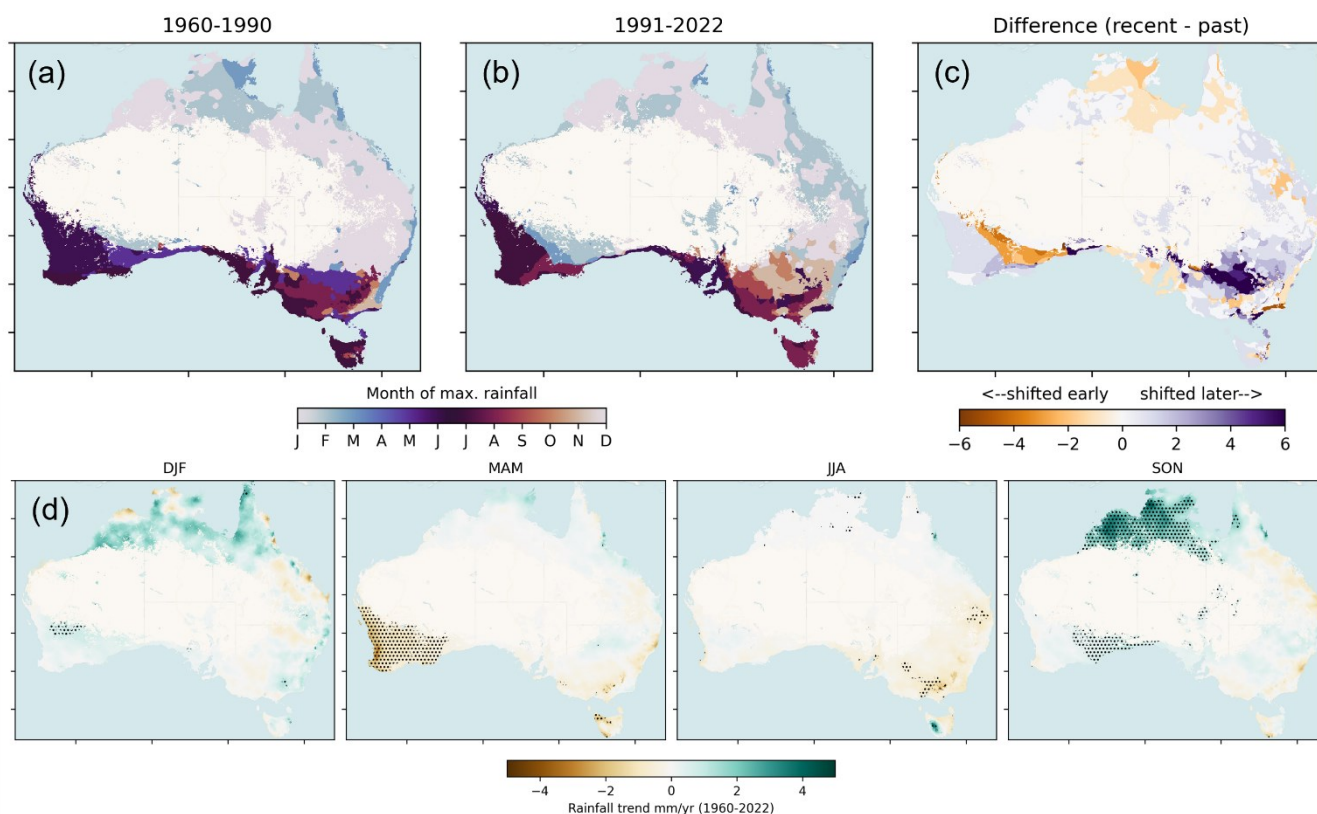


570

**Figure A5: Validation scatter plots and feature importance plots for the gap-filling synthetic NDVI models. a-b) is for the ‘nondesert’ model region which covers the high and low woody cover regions shown in figure 1a, (c-d) is for the ‘desert’ region.**



**575 Figure A6: Distributions of pixel level trends in vPOS (a-e) and POS (f-j), summarised by bioclimatic region (excluding the desert region as most of this region is masked as non-seasonal). ‘M’ refers to the median slope value of the distribution and is indicated by the orange dashed line. Units for vPOS are NDVI per year and units for POS are days per decade.**



580 **Figure A7: Changes to the timing and magnitude of rainfall in Australia.** a) The typical month that rainfall achieves its maximum  
585 value, averaged from 1960-1990. b) Same as (a) but for a 1991-2022 climatology. c) The difference between (a) and (b) where the  
1991-2022 climatology is subtracted from 1960-1990. Orange colours indicate earlier peak rainfall in the more recent climatology  
(in number of months). If peak rainfall shifts from January in 1960-1990 to December in 1991-2022, this is recorded as ‘earlier’  
by one month. Purple colours indicate peak rainfall occurs later in 1991-2022 compared with 1960-1990. If peak rainfall shifts  
from December in 1960-1990 to January in 1991-2022, this is recorded as ‘later’ by one month. d) Theil-Sen trends in the total  
seasonal rainfall from 1960-2022. Hatching indicates significance at 95 % confidence using a Mann-Kendall test.

### Author Contributions.

CB and SR conceived the study, CB performed all analysis and drafted the manuscript. SR, LR, and AVD provided extensive intellectual input and provided extensive edits to the manuscript.

### Competing interests.

590 The authors declare that they have no conflicts of interest.



## Acknowledgements

We thank the National Computing Infrastructure (NCI) for providing a research compute environment without which this work would not be possible.

## Financial Support

595 The first author is supported by a research scholarship provided by Geoscience Australia, funded by the Australian Government.

## References

- Beck, H. E., McVicar, T. R., van Dijk, A. I., Schellekens, J., de Jeu, R. A., and Bruijnzeel, L. A.: Global evaluation of four AVHRR–NDVI data sets: Intercomparison and assessment against Landsat imagery, *Remote Sensing of Environment*, 115, 2547–2563, 2011.
- 600 Beringer, J., Moore, C. E., Cleverly, J., Campbell, D. I., Cleugh, H., De Kauwe, M. G., Kirschbaum, M. U., Griebel, A., Grover, S., and Huete, A.: Bridge to the future: Important lessons from 20 years of ecosystem observations made by the OzFlux network, *Global Change Biology*, 2022.
- Bessenbacher, V., Seneviratne, S. I., and Gudmundsson, L.: CLIMFILL v0.9: a framework for intelligently gap filling Earth observations, *Geosci. Model Dev.*, 15, 4569–4596, 10.5194/gmd-15-4569-2022, 2022.
- 605 Broich, M., Huete, A., Tulbure, M. G., Ma, X., Xin, Q., Paget, M., Restrepo-Coupe, N., Davies, K., Devadas, R., and Held, A.: Land surface phenological response to decadal climate variability across Australia using satellite remote sensing, *Biogeosciences*, 11, 5181–5198, 10.5194/bg-11-5181-2014, 2014.
- Burton, C., Rifai, Sami, Renzullo, Luigi, , & Van Dijk, Albert: AusENDVI: A long-term NDVI dataset for Australia (0.1.0) [dataset], <https://doi.org/10.5281/zenodo.10802704>, 2024.
- 610 Canadell, J. G., Meyer, C., Cook, G. D., Dowdy, A., Briggs, P. R., Knauer, J., Pepler, A., and Haverd, V.: Multi-decadal increase of forest burned area in Australia is linked to climate change, *Nature communications*, 12, 6921, 2021.
- Cawley, G. C. and Talbot, N. L.: On over-fitting in model selection and subsequent selection bias in performance evaluation, *The Journal of Machine Learning Research*, 11, 2079–2107, 2010.
- 615 Chambers, L. E., Altwegg, R., Barbraud, C., Barnard, P., Beaumont, L. J., Crawford, R. J., Durant, J. M., Hughes, L., Keatley, M. R., and Low, M.: Phenological changes in the southern hemisphere, *PLoS one*, 8, e75514, 2013.
- Chen, B.: Comparison of the Two Most Common Phenology Algorithms Imbedded in Land Surface Models, *Journal of Geophysical Research: Atmospheres*, 127, e2022JD037167, 2022.
- Cortés, J., Mahecha, M. D., Reichstein, M., Myneni, R. B., Chen, C., and Breuning, A.: Where are global vegetation greening and browning trends significant?, *Geophysical Research Letters*, 48, e2020GL091496, 2021.
- 620 Donohue, R. J., McVICAR, T. R., and Roderick, M. L.: Climate-related trends in Australian vegetation cover as inferred from satellite observations, 1981–2006, *Global Change Biology*, 15, 1025–1039, 2009.
- Donohue, R. J., Roderick, M. L., McVicar, T. R., and Farquhar, G. D.: Impact of CO<sub>2</sub> fertilization on maximum foliage cover across the globe's warm, arid environments, *Geophysical Research Letters*, 40, 3031–3035, 2013.
- 625 Dusenge, M. E., Duarte, A. G., and Way, D. A.: Plant carbon metabolism and climate change: elevated CO<sub>2</sub> and temperature impacts on photosynthesis, photorespiration and respiration, *New Phytologist*, 221, 32–49, 2019.
- Fensholt, R. and Proud, S. R.: Evaluation of earth observation based global long term vegetation trends—Comparing GIMMS and MODIS global NDVI time series, *Remote Sensing of Environment*, 119, 131–147, 2012.
- 630 Franch, B., Vermote, E. F., Roger, J.-C., Murphy, E., Becker-Reshef, I., Justice, C., Claverie, M., Nagol, J., Csizsar, I., and Meyer, D.: A 30+ year AVHRR land surface reflectance climate data record and its application to wheat yield monitoring, *Remote Sensing*, 9, 296, 2017.
- Frankenberg, C., Yin, Y., Byrne, B., He, L., and Gentine, P.: Comment on “Recent global decline of CO<sub>2</sub> fertilization effects on vegetation photosynthesis”, *Science*, 373, eabg2947, 2021.



- Gerber, F., de Jong, R., Schaepman, M. E., Schaepman-Strub, G., and Furrer, R.: Predicting missing values in spatio-temporal remote sensing data, *IEEE Transactions on Geoscience and Remote Sensing*, 56, 2841-2853, 2018.
- 635 Giglio, L. and Roy, D.: On the outstanding need for a long-term, multi-decadal, validated and quality assessed record of global burned area: Caution in the use of Advanced Very High Resolution Radiometer data, *Science of Remote Sensing*, 2, 100007, 2020.
- Gorman, A. and McGregor, J.: Some considerations for using AVHRR data in climatological studies: II. Instrument performance, *REMOTE SENSING*, 15, 549-565, 1994.
- 640 Haverd, V., Raupach, M. R., Briggs, P. R., Canadell, J. G., Isaac, P., Pickett-Heaps, C., Roxburgh, S. H., van Gorsel, E., Viscarra Rossel, R. A., and Wang, Z.: Multiple observation types reduce uncertainty in Australia's terrestrial carbon and water cycles, *Biogeosciences*, 10, 2011-2040, 10.5194/bg-10-2011-2013, 2013.
- Head, L., Adams, M., McGregor, H. V., and Toole, S.: Climate change and Australia, *Wiley Interdisciplinary Reviews: Climate Change*, 5, 175-197, 2014.
- Hoffmann, A. A., Rymer, P. D., Byrne, M., Ruthrof, K. X., Whinam, J., McGeoch, M., Bergstrom, D. M., Guerin, G. R., Sparrow, B., and 645 Joseph, L.: Impacts of recent climate change on terrestrial flora and fauna: Some emerging Australian examples, *Austral Ecology*, 44, 3-27, 2019.
- Hope, P. K., Drosowsky, W., and Nicholls, N.: Shifts in the synoptic systems influencing southwest Western Australia, *Climate Dynamics*, 26, 751-764, 2006.
- Hopper, S. D. and Gioia, P.: The southwest Australian floristic region: evolution and conservation of a global hot spot of biodiversity, 650 *Annu. Rev. Ecol. Evol. Syst.*, 35, 623-650, 2004.
- Huang, Z., Zhou, L., and Chi, Y.: Spring phenology rather than climate dominates the trends in peak of growing season in the Northern Hemisphere, *Global Change Biology*, 2023.
- Hughes, L.: Climate change and Australia: key vulnerable regions, *Regional Environmental Change*, 11, 189-195, 2011.
- Hutchison, M., Kesteven, J., and Xu, T.: ANUClimate collection [dataset], 2014.
- 655 Krause, C., Dunn, B., Bishop-Taylor, R., Adams, C., Burton, C., Alger, M., Chua, S., Phillips, C., Newey, V., and Kouzoubov, K.: Digital Earth Australia notebooks and tools repository, *Geoscience Australia*, 2021.
- Li, F., Jupp, D. L., Reddy, S., Lymburner, L., Mueller, N., Tan, P., and Islam, A.: An evaluation of the use of atmospheric and BRDF correction to standardize Landsat data, *IEEE Journal of Selected Topics in Applied Earth Observations and Remote Sensing*, 3, 257-270, 2010.
- 660 Li, M., Cao, S., Zhu, Z., Wang, Z., Myneni, R. B., and Piao, S.: Spatiotemporally consistent global dataset of the GIMMS Normalized Difference Vegetation Index (PKU GIMMS NDVI) from 1982 to 2022, *Earth Syst. Sci. Data*, 15, 4181-4203, 10.5194/essd-15-4181-2023, 2023.
- Liao, Z., Van Dijk, A. I., He, B., Larraondo, P. R., and Scarth, P. F.: Woody vegetation cover, height and biomass at 25-m resolution across Australia derived from multiple site, airborne and satellite observations, *International Journal of Applied Earth Observation and 665 Geoinformation*, 93, 102209, 2020.
- Liu, Y., Wu, C., Wang, X., Jassal, R. S., and Gonsamo, A.: Impacts of global change on peak vegetation growth and its timing in terrestrial ecosystems of the continental US, *Global and Planetary Change*, 207, 103657, 2021.
- Lundberg, S. M. and Lee, S.-I.: A unified approach to interpreting model predictions, *Advances in neural information processing systems*, 30, 2017.
- 670 Ma, X., Huete, A., and Tran, N. N.: Interaction of seasonal sun-angle and savanna phenology observed and modelled using MODIS, *Remote Sensing*, 11, 1398, 2019.
- Ma, X., Huete, A., Moran, S., Ponce-Campos, G., and Eamus, D.: Abrupt shifts in phenology and vegetation productivity under climate extremes, *Journal of Geophysical Research: Biogeosciences*, 120, 2036-2052, 2015.
- 675 Ma, X., Huete, A., Yu, Q., Coupe, N. R., Davies, K., Broich, M., Ratana, P., Beringer, J., Hutley, L. B., and Cleverly, J.: Spatial patterns and temporal dynamics in savanna vegetation phenology across the North Australian Tropical Transect, *Remote sensing of Environment*, 139, 97-115, 2013.
- Meyer, H. and Pebesma, E.: Machine learning-based global maps of ecological variables and the challenge of assessing them, *Nature Communications*, 13, 1-4, 2022.
- Moore, C. E., Brown, T., Keenan, T. F., Duursma, R. A., van Dijk, A. I. J. M., Beringer, J., Culvenor, D., Evans, B., Huete, A., Hutley, L. 680 B., Maier, S., Restrepo-Coupe, N., Sonnentag, O., Specht, A., Taylor, J. R., van Gorsel, E., and Liddell, M. J.: Reviews and syntheses: Australian vegetation phenology: new insights from satellite remote sensing and digital repeat photography, *Biogeosciences*, 13, 5085-5102, 10.5194/bg-13-5085-2016, 2016.
- Myers, N., Mittermeier, R. A., Mittermeier, C. G., Da Fonseca, G. A., and Kent, J.: Biodiversity hotspots for conservation priorities, *Nature*, 403, 853-858, 2000.
- 685 O'Donnell, J., Gallagher, R. V., Wilson, P. D., Downey, P. O., Hughes, L., and Leishman, M. R.: Invasion hotspots for non-native plants in a ustralia under current and future climates, *Global Change Biology*, 18, 617-629, 2012.
- Park, T., Chen, C., Macias-Fauria, M., Tømmervik, H., Choi, S., Winkler, A., Bhatt, U. S., Walker, D. A., Piao, S., and Brovkin, V.: Changes in timing of seasonal peak photosynthetic activity in northern ecosystems, *Global change biology*, 25, 2382-2395, 2019.



- 690 Peters, J. M., López, R., Nolf, M., Hutley, L. B., Wardlaw, T., Cernusak, L. A., and Choat, B.: Living on the edge: A continental-scale assessment of forest vulnerability to drought, *Global Change Biology*, 27, 3620-3641, 2021.
- Piao, S., Liu, Q., Chen, A., Janssens, I. A., Fu, Y., Dai, J., Liu, L., Lian, X., Shen, M., and Zhu, X.: Plant phenology and global climate change: Current progresses and challenges, *Global change biology*, 25, 1922-1940, 2019.
- Pinzon, J. E. and Tucker, C. J.: A non-stationary 1981–2012 AVHRR NDVI3g time series, *Remote sensing*, 6, 6929-6960, 2014.
- 695 Pitman, A., Narisma, G., Pielke Sr, R., and Holbrook, N.: Impact of land cover change on the climate of southwest Western Australia, *Journal of Geophysical Research: Atmospheres*, 109, 2004.
- Poulter, B., Frank, D., Ciais, P., Myneni, R. B., Andela, N., Bi, J., Broquet, G., Canadell, J. G., Chevallier, F., and Liu, Y. Y.: Contribution of semi-arid ecosystems to interannual variability of the global carbon cycle, *Nature*, 509, 600-603, 2014.
- Privette, J., Fowler, C., Wick, G., Baldwin, D., and Emery, W.: Effects of orbital drift on AVHRR products: normalized difference vegetation index and sea surface temperature, *Remote Sens. Environ.*, 53, 164-177, 1995.
- 700 Rifai, S. W., De Kauwe, M. G., Ukkola, A. M., Cernusak, L. A., Meir, P., Medlyn, B. E., and Pitman, A. J.: Thirty-eight years of CO<sub>2</sub> fertilization has outpaced growing aridity to drive greening of Australian woody ecosystems, *Biogeosciences*, 19, 491-515, 10.5194/bg-19-491-2022, 2022.
- Schaaf, C. and Wang, Z.: MCD43A4 MODIS/Terra+ aqua BRDF/albedo nadir BRDF adjusted RefDaily L3 global 500 m V006, NASA EOSDIS Land Processes DAAC, 2015.
- 705 Shen, H., Li, X., Cheng, Q., Zeng, C., Yang, G., Li, H., and Zhang, L.: Missing information reconstruction of remote sensing data: A technical review, *IEEE Geoscience and Remote Sensing Magazine*, 3, 61-85, 2015.
- Steffen, W., Sims, J., Walcott, J., and Laughlin, G.: Australian agriculture: coping with dangerous climate change, *Regional Environmental Change*, 11, 205-214, 2011.
- Tian, F., Fensholt, R., Verbesselt, J., Grogan, K., Horion, S., and Wang, Y.: Evaluating temporal consistency of long-term global NDVI datasets for trend analysis, *Remote Sensing of Environment*, 163, 326-340, 2015.
- 710 Tucker, C. J., Pinzon, J. E., Brown, M. E., Slayback, D. A., Pak, E. W., Mahoney, R., Vermote, E. F., and El Saleous, N.: An extended AVHRR 8-km NDVI dataset compatible with MODIS and SPOT vegetation NDVI data, *International journal of remote sensing*, 26, 4485-4498, 2005.
- Ukkola, A. M., Prentice, I. C., Keenan, T. F., Van Dijk, A. I., Viney, N. R., Myneni, R. B., and Bi, J.: Reduced streamflow in water-stressed climates consistent with CO<sub>2</sub> effects on vegetation, *Nature Climate Change*, 6, 75-78, 2016.
- 715 Vermote, E. F., El Saleous, N. Z., and Justice, C. O.: Atmospheric correction of MODIS data in the visible to middle infrared: first results, *Remote Sensing of Environment*, 83, 97-111, 2002.
- Wang, S., Zhang, Y., Ju, W., Chen, J. M., Cescatti, A., Sardans, J., Janssens, I. A., Wu, M., Berry, J. A., and Campbell, J. E.: Response to Comments on “Recent global decline of CO<sub>2</sub> fertilization effects on vegetation photosynthesis”, *Science*, 373, eabg7484, 2021.
- 720 Wang, Z., Wang, H., Wang, T., Wang, L., Liu, X., Zheng, K., and Huang, X.: Large discrepancies of global greening: Indication of multi-source remote sensing data, *Global Ecology and Conservation*, 34, e02016, 2022.
- Xie, Q., Moore, C. E., Cleverly, J., Hall, C. C., Ding, Y., Ma, X., Leigh, A., and Huete, A.: Land surface phenology indicators retrieved across diverse ecosystems using a modified threshold algorithm, *Ecological Indicators*, 147, 110000, 2023.
- 725 Ye, W., van Dijk, A. I., Huete, A., and Yebra, M.: Global trends in vegetation seasonality in the GIMMS NDVI3g and their robustness, *International Journal of Applied Earth Observation and Geoinformation*, 94, 102238, 2021.
- Zeng, C., Shen, H., Zhong, M., Zhang, L., and Wu, P.: Reconstructing MODIS LST based on multitemporal classification and robust regression, *IEEE Geoscience and Remote Sensing Letters*, 12, 512-516, 2014.